Horizontal gene transfer in the human and skin commensal *Malassezia*: a bacterially-derived flavohemoglobin is required for NO resistance and host interaction

Giuseppe Ianiri[1#], Marco A. Coelho[1], Fiorella Ruchti[2], Florian Sparber[2], Timothy J. McMahon[3], Ci Fu[1], Madison Bolejack[4,6], Olivia Donovan[5,6], Hayden Smutney[5,6], Peter Myler[6,7,8], Fred Dietrich[1], David Fox III[4,6], Salomé LeibundGut-Landmann[2], and Joseph Heitman*[1]

[1] Department of Molecular Genetics and Microbiology, Duke University Medical Center, Durham, NC, 27710, USA. [2]Section of Immunology, Vetsuisse Faculty, University of Zürich, Zürich, Switzerland. [3]Department of Medicine, VA Medical Center, Durham, NC, 27705, USA. [4]UCB Pharma, Bainbridge Island, WA, USA; [5]UCB Pharma, Bedford, MA, USA; [6]Seattle Structural Genomics Center for Infectious Disease (SSGCID), Seattle, WA; [7]Center for Global Infectious Disease Research, Seattle Children's Research Institute, Seattle, WA USA; [8]Department of Biomedical Information and Medical Education and Department of Global Health, University of Washington, Seattle, WA USA.

[#]Present address: Department of Agricultural, Environmental and Food Sciences, University of Molise, 86100, Campobasso, Italy

[*]Address correspondence to Joseph Heitman, Department of Molecular Genetics and Microbiology, Duke University Medical Center, Durham, North Carolina, United States of America. Phone +1 (919) 684-2824. Fax (919) 684-2790. Email heitm001@duke.edu.

Abstract

The skin of humans and animals is colonized by commensal and pathogenic fungi and bacteria that share this ecological niche and have established microbial interactions. *Malassezia* are the most abundant fungal skin inhabitant of all warm-blooded animals, and have been implicated in skin diseases and systemic disorders, including Crohn's disease and pancreatic cancer. Flavohemoglobin is a key enzyme involved in microbial nitrosative stress resistance and nitric oxide degradation. Comparative genomics and phylogenetic analyses within the *Malassezia* genus revealed that extant flavohemoglobin-encoding genes are present as single copy in different species, but were acquired through independent horizontal gene transfer events from different donor bacteria that are part of the mammalian microbiome. Through targeted gene deletion and functional complementation in *M. sympodialis*, we demonstrated that both bacterially-derived flavohemoglobins are cytoplasmic proteins required for nitric oxide detoxification and nitrosative stress resistance under aerobic conditions. RNAseq analysis revealed that endogenous accumulation of nitric oxide resulted in upregulation of genes involved in stress responses, and downregulation of the MalaS7 allergen-encoding gene. Solution of the high-resolution X-ray crystal structure of *Malassezia* flavohemoglobin revealed features conserved with both bacterial and fungal flavohemoglobins. *In vivo* pathogenesis is independent of *Malassezia* flavohemoglobin. Lastly, we identified additional 30 genus- and species- specific horizontal gene transfer candidates that might have contributed to the evolution of this genus as the most common inhabitants of animal skin.

Introduction

The skin microbiome includes numerous microorganisms that establish a variety of direct and indirect interactions characterized by the exchange of genetic material that impact microbial biology contributing to their speciation and evolution. *Malassezia* is the most abundant fungal genus resident on the skin of all warm-blooded animals, representing more than 90% of the skin mycobiome[1]. This genus presently consists of 18 diverse species[2], each with an unusually compact genome[3]. Although commensals, *Malassezia* species are also associated with a number of clinical skin disorders, including pityriasis versicolor, dandruff, and atopic dermatitis (AD)[4]. A recently-developed epicutaneous murine model revealed that the host responses to *Malassezia* are dominated by pro-inflammatory cytokine IL-17 and related factors that prevent fungal overgrowth and exacerbate inflammation under atopy-like conditions[5]. Furthermore, *Malassezia* species have also been implicated recently as causal agents of Crohn's Disease/Inflammatory Bowel Disease in patients with *CARD9* mutations, and in accelerating the progression of Pancreatic Adenocarcinoma in murine models and in humans[6,7].

Nitric Oxide (NO) is a reactive compound of central importance in biological systems. While little is known about NO synthesis in fungi, in mammals NO is synthesized by NO synthases (NOS isoforms), and NO functions as a signaling molecule and biomolecule modifier affecting various cellular processes. Imbalance in cellular NO levels leads to altered redox homeostasis, resulting in the production of reactive nitrogen species (RNS) responsible for nitrosative stress[8,9]. Type I flavohemoglobin constitutes the main enzyme deployed by microbes to counteract NO toxicity by converting it to inert nitrate, a source of nitrogen, via the NO-dioxygenation reaction[8,9]. A type II flavohemoglobin has also been identified in *Mycobacterium tuberculosis* and other actinobacteria, but it lacks NO consuming activity and it utilizes D-lactate as an electron donor to mediate electron transfer[10,11]. Evolution of flavohemoglobins in microbes has been previously investigated[12-14], revealing a dynamic distribution across bacteria and eukaryotes characterized by frequent gene loss, gene duplication, and horizontal gene transfer (HGT) events. An interesting finding of these phylogenetic studies was the HGT-mediated acquisition of a bacterial flavohemoglobin encoding gene *YHB1* by *M. globosa* and *M. sympodialis*[12,13].

In this study we employed molecular, biochemical, and structural analyses to demonstrate that the HGT of the bacterial flavohemoglobin in *Malassezia* resulted in a gain of function

critical for resistance to nitrosative stress and detoxification of NO under aerobic conditions. Moreover, analysis of the available *Malassezia* genomes revealed that extant flavohemoglobin-encoding genes are present as a single copy in different species, and phylogeny inference suggest that they originated from different donor bacteria through independent horizontal gene transfer events. Through trans-species complementation we demonstrated that the second bacterially-derived flavohemoglobin identified, Yhb101, restore resistance of the *yhb1*Δ mutant to nitrosative stress-inducing agents and also is able to consume NO. RNAseq analysis revealed that endogenous accumulation of nitric oxide results in upregulation of genes involved in stress responses and transport, and downregulation of the allergen-encoding genes. The characterization of the X-ray structure of the *Malassezia* flavohemoglobin revealed features shared with bacterial and fungal flavohemoglobins. Moreover, the *Malassezia* flavohemoglobin mutant displayed modest survival within host macrophages, but we did not find evidence that suggested an involvement of flavohemoglobin on survival on the skin or in the GI tract. Lastly, we identified 30 additional genus- and species-specific HGT events, with the donors being predominantly Actinobacteria and Proteobacteria. Similar to *Malassezia*, these donor species are some of the most common members of human and mammal microbiomes, suggesting that niche overlap may have enhanced the opportunity for inter-kingdom HGT.

Results

***Malassezia* flavohemoglobin-encoding genes have been acquired from bacteria through independent HGT events.** Flavohemoglobins are critical for nitric oxide (NO) detoxification and counteract nitrosative stress[9]. Previous studies reported that the flavohemoglobin-encoding gene *YHB1* was acquired by *M. globosa* and *M. sympodialis* through HGT from *Corynebacterium*, a bacterial genus within the Actinobacteria that includes species that are part of the human microbiome[12,13].

Because flavohemoglobins are widespread in both bacteria and eukaryotes, we examined whether the remaining 13 sequenced *Malassezia* species also contain a flavohemoglobin-encoding gene, and whether it had a fungal or bacterial origin. BLAST analyses with the *M. globosa* Yhb1 sequence as query identified a single copy of *YHB1* in all *Malassezia* species. Intriguingly, this comparative search revealed that the best hits in *M. yamatoensis* and *M. slooffiae* had lower *E*-values (5e-64 and 1e-59, respectively) compared to the remaining *Malassezia* species (*E*-values ranging from 0.0 to 7e-161), possibly suggesting different origins or modifications of these flavohemoglobin-encoding genes. To elucidate the evolutionary trajectory of flavohemoglobin within the whole *Malassezia* genus, a Maximum Likelihood (ML) phylogenetic tree was reconstructed using >2000 Yhb1 bacterial and fungal sequences retrieved from GenBank. This phylogenetic analysis revealed two clades of flavohemoglobin within *Malassezia* genus: clade 1 that includes 13 species and clusters together with *Brevibacterium* species belonging to Actinobacteria; and clade 2 that includes *M. yamatoensis* and *M. slooffiae* and clusters together with different Actinobacteria with the closest relative being *Kocuria kristinae* (Fig. 1 A-C). To evaluate the statistical phylogenetic support for the two *Malassezia* flavohemoglobin clades whose distribution was not monophyletic, we performed approximately unbiased (AU) comparative topology tests. The constrained ML phylogeny, in which all *Malassezia* flavohemoglobins were forced to be monophyletic was significantly rejected (AU test, *P* value = 0.001, Fig. 1D), thus not supporting the null hypothesis that all flavohemoglobin genes in *Malassezia* have a single origin.

To validate this further, a region of ~30 kb surrounding the flavohemoglobin encoding gene in all sequenced *Malassezia* species was subjected to synteny comparison (Fig. 1E-F). Overall this region was highly syntenic across species, with the exception of some lineage-

specific rearrangements located upstream of *YHB1* (Fig. 1F). Remarkably, while the same regions were also highly conserved in *M. yamatoensis* and *M. slooffiae*, they both lacked the flavohemoglobin-encoding gene, which is instead located in a different, non-syntenic, regions of their genomes (Fig. 1F and Fig. S1). Therefore, both phylogenic and synteny comparisons strongly support the hypothesis that *Malassezia* flavohemoglobin genes were acquired through independent HGT events from different bacterial donor species. We named the flavohemoglobin of clade 1 Yhb1 following the *S. cerevisiae* nomenclature[15], and that of *M. yamatoensis* and *M. slooffiae* Yhb101 (clade 2). The two different flavohemoglobins protein sequences share 38% identity (Fig. S2).

Because several studies suggest that genomic regions flanking horizontally-acquired genes are enriched in DNA transposons and retrotransposons[16,17], a 5 kb region surrounding the flavohemoglobin-encoding genes was analyzed in two *Malassezia* species representative of clade 1 (*M. sympodialis*) and clade 2 (*M. slooffiae*). Dot plot comparisons revealed overall high co-linearity with the common flanking genes encoding a hypothetical protein and Nsr1 (Fig. S3A). Interestingly, a highly repetitive sequence that shares similarity with the long terminal repeat (LTR) Gypsy was identified in the *NSR1* gene flanking *YHB1* (Fig. S3A-B), and we speculate that this LTR-like region might have facilitated the non-homologous end joining (NHEJ) integration of the bacterial *YHB1* gene into the *Malassezia* common ancestor.

The flavohemoglobin-encoding gene *YHB101* in *M. yamatoensis* and *M. slooffiae* seems to have been acquired from the same bacterial donor lineage (Fig. 1A-C), although its genomic location is not syntenic in these two species (Fig. 1E-F). In particular, *M. slooffiae YHB101* is located in a region that is otherwise highly conserved across *Malassezia* (Fig. S1A-B), and is devoid of transposable elements or repetitive regions that could facilitate NHEJ of *YHB101* (Fig. S1B). In contrast, *M. yamatoensis YHB101* located at the end of a chromosome and its adjacent genes are not syntenic in other *Malassezia* species, with the exception of a more distant group of five genes (from *JLP1* to *MSS1*) (Fig. S1C). In other *Malassezia* species (eg *M. japonica, M. slooffiae, M. sympodialis*) these five genes are subtelomeric, suggesting that chromosomal rearrangement might have contributed to generate the unique rearrangement of genes surrounding *M. yamatoensis YHB101* (Fig. 1E; Fig. S1C).

Based on the analyses performed and on the availability of *Malassezia* genomes, we propose the following evolutionary model of flavohemoglobin-mediated HGT in *Malassezia*: 1)

a *Malassezia* common ancestor acquired the *YHB1* gene via HGT from a *Brevibacterium*-related donor; 2) *M. yamatoensis* and *M. slooffiae* subsequently acquired the *YHB101* gene from a different bacterial donor lineage (*Kocuria*) via HGT, concomitant with the loss of the *YHB1* gene; 3) chromosomal rearrangements relocated *YHB101* in *M. yamatoensis* to a subtelomeric location.

Bacterially-derived flavohemoglobin-encoding genes are required for nitrosative stress resistance and NO detoxification in *Malassezia*. Flavohemoglobins are critical for nitric oxide (NO) detoxification and counteract nitrosative stress[9]. To assess whether this HGT event in *Malassezia* resulted in a gain of function, we deleted the *YHB1* ORF (MSYG_3741) of *M. sympodialis* ATCC42132 through targeted mutagenesis using our recently developed transformation protocol based on transconjugation mediated by *Agrobacterium tumefaciens*[18,19] (Fig. S4A). *M. sympodialis yhb1*Δ targeted deletion mutants were identified by PCR using primers designed outside the region involved in homologous recombination and with *NAT* specific primers (Fig. S4A).

The *M. sympodialis yhb1*Δ mutant exhibits hypersensitivity to the NO-donors DetaNONOate and sodium nitrite ($NaNO_2$) but not to hydrogen peroxide (H_2O_2) (Fig. 2A). The two identified *Malassezia* flavohemoglobins Yhb1 and Yhb101 were used to generate GFP fusion proteins whose expression was driven by the respective endogenous promoter and terminator to complement the *M. sympodialis yhb1*Δ mutant phenotype and to assess protein localization (Fig. S4B). Reintroduction of either flavohemoglobin in the *M. sympodialis yhb1*Δ mutant restored resistance to nitrosative stress at the WT level (Fig. 2A). In agreement, fusion protein expression in complemented strains was confirmed both by qPCR (Fig. S4C-D) and fluorescence microcopy imaging of GFP expression, which revealed that *Malassezia* flavohemoglobins are cytoplasmic (Fig. 2B). A GFP-Yhb1 fusion protein cloned under the control of the histone *H3* promoter and terminator (Fig. S4B) was less effective in complementing the *yhb1*Δ mutant phenotype (data not shown).

Next we tested whether the yeast flavohemoglobin was able to actively detoxify NO, which could potentially account for its involvement in nitrosative stress resistance. To this aim, we adapted a biochemical assay used for evaluating NO consumption in red blood cells and plasma[20] to the commensal yeast *Malassezia* (File S2). As shown in Figure 2C, while the *M.*

sympodialis WT strain exhibited robust and dose-dependent NO degradation, the *yhb1*Δ mutant showed no NO consumption. Complemented strains were able to actively consume NO, although *M. sympodialis yhb1*Δ + *YHB101-GFP* displayed a lower NO consumption, corroborating the results of the phenotypic assay, GFP expression, and FACS analysis (Fig. 2A-C). These differences might be due to less efficient cross-species complementation of the *M. yamatoensis* Yhb101-GFP fusion protein in the *yhb1*Δ mutant of *M. sympodialis*, which was a strategy chosen because of the lack of protocols for gene deletion in *M. slooffiae* and *M. yamatoensis*. Taken together these genetic and biochemical analyses show that the bacterially-derived flavohemoglobin protect *Malassezia* from nitrosative stress by decreasing toxic levels of NO.

To assess intracellular production of NO by *M. sympodialis*, cells were stained with the NO-specific dye 4-Amino-5-methylamino- 2□,7□-diaminofluorescein diacetate (DAF-FM DA), which passively diffuses across membranes and emits increased fluorescence after reacting with NO. Fluorescent microscopy revealed intracellular accumulation of NO in both the WT and *yhb1*Δ mutant of *M. sympodialis* (Fig. 2D). NO-staining was quantified by FACS analysis, revealing significantly higher NO accumulation in the flavohemoglobin mutant *yhb1*Δ compared to the *M. sympodialis* WT (Fig. 2E-F). Because DAF-FM DA and GFP have similar excitation/emission spectra, complemented strains could not be tested for NO accumulation via flow cytometry, and therefore an independent *M. sympodialis yhb1*Δ mutant was tested and yielded similar results. These results indicate that the lack of a functional flavohemoglobin leads to intracellular accumulation of NO.

Finally, a broader analysis was performed to assess other functions of the *Malassezia* flavohemoglobins in response to a variety of environmental stresses and clinical antifungals, but in all cases the *M. sympodialis yhb1*Δ mutant phenotype was not significantly different from the WT (Fig. S5). Several studies also report the protective role of both bacterial and fungal flavohemoglobins against NO under anaerobic conditions[9,15,21]. However, we could not confirm this function for the *Malassezia* flavohemoglobin in our anaerobic experiment (Fig. S6).

A recent inactivation of *YHB1* in *M. nana* results in compromised NO enzymatic consume. Analysis of Yhb1 protein prediction across species revealed that *M. nana YHB1* underwent pseudogenization following a G-to-T transversion in the glycine codon GGA, generating a premature TGA stop codon at the 29th amino acid (Fig. S7A). Literature search revealed that the

sequenced strain of *M. nana* CBS9557 was isolated in Japan from a cat with otitis externa[22], while the other four known *M. nana* strains were collected in Brazil: *M. nana* CBS9558 and CBS9559 from cows with otitis externa, and CBS9560 and CBS9561 from healthy cows[22].

The *M. nana* strains CBS9557, CBS9559, and CBS9560 were used to investigate whether the pseudogenization event occurred in a *M. nana* ancestor, and whether it impacts nitrosative stress resistance and NO consumption. Because no genomes are available for the *M. nana* strains CBS9559 and CBS9560, their *YHB1* gene was amplified by PCR and Sanger sequenced using primers designed on the *YHB1* of *M. nana* CBS9557. *YHB1* sequence comparison confirmed a premature stop codon present in only CBS9557, with both Brazilian *M. nana* isolates having a full-coding *YHB1* gene (Fig. S7A). Phenotypic analysis revealed no significant difference in resistance to nitrosative stress by the three *M. nana* strains, with only a modestly increased sensitivity displayed by CBS9557 exposed to sodium nitrite (Fig. S7B). Strikingly, *M. nana* CBS9557 displayed undetectable NO consumption activity as obtained for the *M. sympodialis* *yhb1*Δ mutant, while *M. nana* CBS9559 and CBS9560 showed normal NO consumption (Fig. S7C). These data suggest that the non-functional of flavohemoglobin in *M. nana* CBS9557 impaired the ability to consume NO, but this does not impact the resistance to nitrosative stress, which might be compensated by other stress responsive pathways.

Intriguingly, another pseudogenization event of a bacterial gene encoding an aliphatic amidase was also identified in *M. nana* CBS9557. These nonsense mutations were identified only in the *M. nana* CBS9557 isolated in Japan, suggesting that the different origin of the *M. nana* strains might contribute to this intraspecies diversity. This hypothesis is further supported by different phenotypic traits displayed by the *M. nana* isolates (Fig. S8). Exposure to several stress conditions revealed different responses to the most common antifungal drugs by *M. nana* strains, with strain CBS9557 displaying increased sensitivity to amphotericin B and resistance to fluconazole, and the geographically-related strains CBS9559 and CBS9560 displaying an opposite phenotype (Fig. S8).

NO accumulation in *M. sympodialis* leads to downregulation of predicted pathogenicity factors. Because the *M. sympodialis* flavohemoglobin mutant *yhb1*Δ accumulates higher amounts of NO than the WT (Fig. 2 D-E), we compared their transcriptomic profile to elucidate any potential signaling role of endogenous NO. RNAseq analysis revealed 36 differentially

expressed genes for FDR<0.05, of which 14 were upregulated and 22 were downregulated; using an additional threshold of log_2FC +/- 0.5 we found 3 upregulated and 9 downregulated genes (Fig. 3A; Tables S1-S2). The only upregulated gene with $log_2FC > 1$ encodes an uncharacterized protein (MSYG_1280), while two others with $log_2FC < 1$ encode Nop56 (or Sik1), a nucleolar protein involved in pre-rRNA processing, and an uncharacterized protein (MSYG_0148) predicted to be involved in magnesium transport. Other known upregulated genes with $log_2FC <$ 0.05 are involved in response to stresses and transport (Table S1). The majority of downregulated DEGs include those encoding hypothetical proteins (6 out of 9), the regulator of phospholipase D Sfr1, two MalaS7 allergens, and an uncharacterized allergen. It is worth noting that a large number of differentially expressed genes (DEGs) are predicted to encode unknown proteins, suggesting novel and unknown signaling pathways regulated by endogenous NO in *Malassezia* (Table S1-S2).

Next, to elucidate the global transcriptomic response of *M. sympodialis* exposed to nitrosative stress, RNAseq analysis for *M. sympodialis* WT cells treated with the NO-generating agent sodium nitrite was performed. Compared to the untreated control, 112 genes were upregulated and 50 were downregulated (FDR<0.05; log_2FC +/- 0.5) (Fig. 3B). The most represented classes of upregulated genes include those involved in stress resistance, cellular detoxification and transport, and metabolism. The most expressed genes included *HEM1* involved in the heme biosynthetic process, *DAL2*, *DAL4* and *DCG1* involved in nitrogen metabolism, *RAD57* involved in DNA repair, the general amino acid permease *GAP1*, an uncharacterized lipase, and an uncharacterized oxidoreductase. The flavohemoglobin-encoding gene *YHB1* was significantly upregulated for false discovery rate (FDR) <0.05, but it had low expression level ($log_2FC = 0.33$). Lower expression of *YHB1* was also observed in *S. cerevisiae* cells exposed to nitrosative stress[23], although its role in NO consumption has been well characterized[15]. Four transcription factors were upregulated (*HSF1, UPC2, BAS1* and *HMS1*), and the heat shock transcription factor Hsf1 might be the key candidate that activates nitrosative stress responsive genes (Table S3), given its known role in response to stresses in other fungi[24,25].

The most represented GO category of downregulated genes encodes integral components of membrane, which includes transporters and putative *Malassezia* allergens; other downregulated genes are involved in calcium metabolism, protein folding, and proteolysis. Two

transcription factors were downregulated, and they include the pH responsive Rim101, and an uncharacterized bZIP transcription factor (Fig. 3C, Table S4).

Comparison of the two different RNAseq dataset revealed two common upregulated genes, encoding the glycerol dehydrogenase Gcy1 and the catalase Cta1, and 10 downregulated genes that include 4 *Malassezia* allergens, a putative secreted lipase, and 5 hypothetical proteins (Fig. 3D). While it is not surprising to find upregulation of a detoxifying enzyme such as catalase, it is intriguing to find downregulation of genes encoding predicted pathogenicity factors.

***Malassezia* flavohemoglobin has characteristic features of both bacterial and fungal flavohemoglobins.** We hypothesized that if a protein is acquired by HGT its structure will likely remain fairly similar to that of the donor organism in order to retain its original function. Attempts to resolve the crystal structures of both *Malassezia* flavohemoglobins were carried out, but only the *M. yamatoensis* flavohemoglobin Yhb101 formed crystals to be analyzed. The structure was determined *de novo* by SAD phasing off the heme-iron bound to the globin domain of the protein (Table S5). The flavohemoglobin structure is highly conserved with previously characterized structures of this enzyme family and consists of an N-terminal globin domain coordinating an iron-bound (Fe^{2+}) heme and a C-terminal reductase domain with both FAD- and NAD-binding sub-domains, of which only FAD is bound (Fig. 4A). An overlay of a flavohemoglobin structure from *E. coli* and *S. cerevisiae* on the *M. yamatoensis* crystal structure highlights conserved binding sites between the proteins (Fig. 4B). Alignment of the globin domains between literature and experimental structures resulted in an RMSD value of 1.532Å for *E. coli* and 1.434Å for *S. cerevisiae*, mostly resulting from slight shifts in the D-loop and E-helix between the structures compared. Common among all of the structures analyzed is the histidine residue coordinating with the heme iron from the proximal side. This member of the catalytic triad is supported by tyrosine (Tyr98) and glutamate (Glu140) residues conserved in sequence and structure between bacterial, and fungal/yeast flavohemoglobins[26,27]. In *M. yamatoensis*, as also observed in *E. coli*, the heme iron is ligated by 5 atoms: 4 from the heme and His88 from the F-helix. Substrates commonly bind on the distal side of the heme and lead to a conformational change in the planarity of the heme molecule. The E-Helix on the distal side of the heme molecule contributes Leu58, a conserved residue which approaches the heme-bound iron from 3.7Å away. At this position, the 6th coordination site for the iron is occluded, again similar to the

E. coli crystal structure, but unlike the yeast structure where a three-atom small molecule co-crystallized. In addition, Tyr29 and Gln53, shown to be important in coordination of ligands and the heme, respectively, are conserved in sequence and structure.

In *M. yamatoensis* Yhb101, the D-loop acts as a bridge between the C- and E-helices and the interface between the bound FAD and heme. Comparison of the D-loops from these structures shows the *M. yamatoensis* D-loop adopts a nearly identical helical structure as that of *S. cerevisiae*, in contrast to the *E. coli* D-loop**,** which is more extended. The *M. yamatoensis* E-helix also adopts a ~30° bend immediately following Leu58, which may straighten out once a substrate is bound. This structural adjustment likely communicates substrate binding near the heme to the reductase domain through movements in the D-loop as the heme B pyrrole proprionate forms a hydrogen bond with the main-chain NH of Ser45, the first residue in the D-loop (Figure S9). The neighboring propionate group forms two hydrogen bonds, directly with the side-chain of Arg83 (F-Helix) and indirectly through water with the primary amine of Lys87. A water network can also be traced to the main-chain carbonyl of Phe381, which is positioned above the FAD isoalloxazine ring, protecting it from NAD binding, a conserved feature across all flavohemoglobin structures in the closed state. The FAD sits within the conserved linker region of the protein and binds to both the globin-binding moiety and the flavin-binding moiety. The FAD for *M. yamatoensis* shows a rotation about the second phosphate in comparison to *E. coli* and *S. cerevisiae*, which results in displacement of the adenine ring but only a slight shift of the flavin group. Lastly, the C-terminus of *M. yamatoensis* demonstrates a conformational change when compared to the other organisms. Previous flavohemoglobin structures have shown an α-helix through the C-terminus; however, these residues appear to lack this organized structure.

The *Malassezia* flavohemoglobins were aligned with those of the closer HGT donor bacteria *B. ravenspurgense, K. kristinae, R. nasimurium,* and with the model yeast *S. cerevisiae* (File S3). Most of the known functional regions were conserved in both the *Malassezia* Yhb1 and Yhb101, with the notable differences being the lack of conserved tyrosine (Y126) residues in the hydrogen bond in *M. vespertilionis, M. japonica, M. obtusa* and *M. globosa*. Other variations were also found in the cofactor binding sites of the reductase domain, in particular, 1) the isoalloxazine FAD binding site was different between the two *Malassezia* flavohemoglobin, with RQYS being the Yhb1 motif, in common also with other bacterial flavohemoglobins (*E. coli* and

Salmonella)[9], and RQFT being that of the Yhb101, which is also shared with the putative donor bacteria (*K. kristinae*); and 2) the nicotinamide adenine dinucleotide (NADH) motif being GIGXT for Yhb1, and GIGVT for Yhb101 (File S3).

***Malassezia* flavohemoglobins are not required for survival on the host.** Previous studies in human fungal pathogens indicate that flavohemoglobins are required for pathogenesis[28,29]. In our experiments we found that *M. sympodialis* WT, *yhb1*Δ mutant, and *yhb1*Δ + *YHB1* and *yhb1*Δ + *YHB101* complemented strains have similar levels of survival within activated macrophages (Fig. 5A-B). This result is in contrast with previous findings in *C. neoformans*[28], but it corroborates results obtained in *A. fumigatus*[30]. Further, the recently developed murine model for *Malassezia* skin infection[5] was utilized to test pathogenicity of the flavohemoglobin strains and the induction of host response. Corroborating ex vivo data, we found no differences both in terms of host tissue colonization and host inflammatory response for the *yhb1*Δ mutant compared to the complemented strains (Fig. 5C-E, Fig. S8). In agreement, there were no differences between WT and *Nos2-/-* mice when challenged with *M. sympodialis* WT (Fig. 5F-H, Fig. S10). These results suggest that flavohemoglobin is not required for pathogenesis of *Malassezia* in an experimental skin model.

Lastly, several attempts were also carried out to test survival of *M. sympodialis* WT and flavohemoglobin strains within the GI tract of WT and *Nos2*-/- mice. Because of the high amount of NO produced in the GI tract of mice during inflammation[31], and the recently-reported involvement of *Malassezia restricta* in Crohn disease[6], we hypothesized that the flavohemoglobin would be required for *M. sympodialis* survival in GI tract during inflammation. We followed the protocol developed for GI tract colonization by *M. restricta*[6], but unfortunately we could never recover any *M. sympodialis* colony. For this reason, whether *Malassezia* flavohemoglobin is required for survival within the GI tract could not be determined.

Analysis of *Malassezia* genomes revealed extensive HGT events from bacteria. Given the gain of function due to acquisition of the bacterially-derived flavohemoglobins by *Malassezia* species, we sought to identify additional HGT candidate genes in the *Malassezia* genus. In a previous study, 8 HGT events were identified in *M. sympodialis*, and then their presence was assessed in other species within the genus[3]. In the present study we applied a previously

described analytical pipeline[32] based on three HGT metrics - the HGT index[33], the Alien Index (AI)[34] and the Consensus Hit Support (CHS)[35] - to identify novel genus and species-specific HGT events. Our goal was not to explicitly establish the evolutionary history of individual genes, but rather to estimate bacteria-derived HGT candidates for the complete set of *Malassezia* genomes. Besides recovering the *YHB1* and *YHB101* genes as an HGT candidate, this analysis identified in addition a total of 30 HGT candidate genes (Fig. 6 and Table S6), seven of which in common with the previous study. HGT candidates found in the majority of the *Malassezia* species include genes involved in broad oxidative stress resistance, such as catalase and oxidoreductases, found in some cases in multiple copies. Other examples include a deoxyribodipyrimidine photo-lyase predicted to be involved in repair of UV radiation-induced DNA damage, and a class I SAM-dependent methyltransferase potentially modifying a variety of biomolecules, including DNA, proteins and small-molecule secondary metabolites. Another interesting HGT candidate is the gene encoding a septicolysin-like protein, which is known as a pore-forming bacterial toxin that might play a role as virulence factor[36,37]. This gene is absent in all *Malassezia* species phylogenetically related to *M. sympodialis*, and is present as five copies in *M. globosa*. Furthermore, a large number of HGT events unique to *Malassezia* species of clade A were found, and the acquired genes encode a variety of proteins with different functions, such as hydrolysis, protein transport and folding, detoxification of xenobiotics, and resistance to stresses. Finally, 12 of the HGT candidates identified were unique to certain *Malassezia* species. An intriguing case is *M. japonica* for which we found four unique HGT candidates, one of them found in 3 copies. These genes encode orthologs of the fungal Gre2 protein, which is known to be involved in responses to a variety of environmental stresses[38,39].

Discussion

In the present study we report the functional characterization of two *Malassezia* flavohemoglobin encoding genes that were independently acquired through HGT from different Actinobacteria donors. Our experimental analyses demonstrate that both bacterially-derived flavohemoglobins are involved in nitrosative stress resistance and NO degradation, consistent with its known functions in bacteria and fungi[9].

Although the mechanisms of HGT in fungi are not fully understood, several possible mechanisms have been reported [16,40]. One such mechanism is gene acquisition through

conjugation, which requires contact between bacterial donor and fungal recipient[40]. For the HGT events that mediated flavohemoglobin acquisition by *Malassezia*, the closest phylogenetic donors are Actinobacteria that are part of the mammalian microbiome and hence share the same ecological niche with *Malassezia*. A dilemma that is common to all HGT events is that if a gene is required for survival in a certain condition, its transfer in that condition is in theory unfeasible[41]. Because NO is synthesized by the mammals, including by the skin[42], we speculated that NO presence enhanced the HGT transfer of bacterial flavohemoglobin(s) to a fungal *Malassezia* ancestor that acquired the ability to actively consume NO.

Noteworthy, a large number of eukaryotic organisms including fungi lack a flavohemoglobin-encoding gene, suggesting the existence of alternative pathways for nitrosative stress resistance and NO utilization. For example, in *Histoplasma capsulatum*, the etiologic agent of histoplasmosis, Yhb1 is replaced by a P450-type NO reductase[43], whereas in other cases, such as for the basidiomycetous fungi *Moniliellia*, *Ustilago*, and *Puccinia*, NO metabolism in the absence of flavohemoglobin has yet to be elucidated. The evolution and diversification of flavohemoglobin-encoding genes has been complex and has been characterized by several prokaryote-prokaryote and prokaryote-eukaryote HGT events[13], hence suggesting its significant contribution for habitat colonization by a species but likely a dispensable role in evolutionary divergence.

Is the bacterial flavohemoglobin required for *Malassezia* interaction with the host? While a number of studies in bacteria and fungi reported a role for flavohemoglobin in microbial pathogenesis[9], we surprisingly found that *Malassezia* flavohemoglobins are dispensable for survival within macrophages and for skin infection in our experimental conditions. Conversely, we propose that *Malassezia* flavohemoglobins are important for the commensal lifestyle of *Malassezia* through regulation of NO homeostasis, a hypothesis corroborated by downregulation of putative virulence factors (ie allergens and lipases) in our transcriptomic analyses.

Analysis of *Malassezia* genomes revealed a large number of HGT events, suggesting their substantial contribution in *Malassezia* evolution, speciation, and niche adaptation. Donor bacteria include those that are part of the microbiota of animals, but also others that are known to inhabit a variety of terrestrial and marine habitats, raising questions about a possible wider

environmental distribution of a *Malassezia* ancestor. This could be correlated with the presence of *Malassezia* DNA in a number of unexpected areas, such as in association with corals and sea sponges in the ocean[44]. Moreover, most of the HGT candidate genes identified in *Malassezia* operate as a self-contained metabolic units, which has been proposed to facilitate HGT[13]. Intriguingly, the high number of HGT events suggests also a predisposition of *Malassezia* to bacterial conjugation, in line with our previous findings that *A. tumefaciens*-mediated transformation is the only effective technique for molecular manipulation of *Malassezia*[18]. There are a number of identified HGT that are predicted to be important for *Malassezia* pathophysiology and that can be characterized using the methodologies reported in the present study.

Materials and Methods

Strains used in the present study. The *M. sympodialis* strains ATCC42132 was utilized as a model species for genetic manipulations. In addition, *M. slooffiae* CBS7856, *M. yamatoensis* CBS9725, and *M. nana* strains CBS9557, CBS9559, and CBS9560 were employed for NO consumption assays. These strains were grown on modified Dixon's media (mDixon), which is the medium routinely used for culturing *Malassezia* species[3].

Identification of *YHB1* genes in *Malassezia* genomes and synteny analyses. Protein-coding sequences were obtained using the *ab initio* gene predictor AUGUSTUS v3.2.2[45] for each *Malassezia* species that lacked a genome annotation (as of September 2017). To search for *YHB1* homologs, local BLAST databases were set up for both the genome assemblies and the translated coding sequences, and the *M. globosa* Yhb1 protein sequence (GenBank XP_001730006.1) was queried against each database using BLASTP or TBLASTN. Top BLAST-identified protein sequences were retrieved, and the presence of the typical FHbs domains, consisting of an N-terminal globin domain fused with a C-terminal FAD- and NAD-binding oxidoreductase modules, were inspected using InterProScan 5[46]. For the analysis of relative gene-order conservation (synteny) between *Malassezia* species, a region of ~ 32 kb surrounding the *YHB1* gene (~7-8 genes on each side) was carefully examined and compared using top scoring BLASTP against the reference genome annotations of *M. sympodialis*, *M. globosa* and *M. pachydermatis*.

Yhb1 phylogeny and topology tests. The *Malassezia globosa* Yhb1 protein was queried against the Genbank non-redundant (nr) protein database (last accessed in August 2017) with BLASTP

and an e-value inclusion threshold of 1e-10. Protein sequences corresponding to the top 5000 hits were extracted and utilized for downstream analyses. In addition, all putative *Malassezia* Yhb1 proteins identified from the genome data, as well as the functionally characterized Yhb1 gene of *S. cerevisiae*, were included in the dataset. Highly similar sequences were collapsed with CD-HIT v4.7[47] using a sequence identity threshold of 0.95 (-c 0.95) and word length of 5 (-n 5) to remove redundancy and correcting the bias within the dataset. Sequences were aligned with MAFFT v7.310 using the FFT-NS-i strategy[48] and poorly aligned regions were trimmed with TrimAl v1.4. (-gappyout)[49]. The Yhb1 phylogenetic tree was constructed using IQ-TREE v1.5.5[50] and the LG+F+I+G4 amino acid model of substitution as determined by ModelFinder[51]. Because the dataset consisted of a large number of relatively short sequences, we reduced the perturbation strength (-pers 0.2) and increased the number of stop iterations (-nstop 500) during tree search. Branch support was accessed with the ultrafast bootstrap approximation (UFboot)[52] and the SH-like approximate likelihood ratio (SH-aLRT) test[53] both with 10,000 replicates (-bb 10000 –alrt 10000). Tests of monophyly were performed in CONSEL version 1.2[54] using the approximately unbiased (AU) test[55] to determine whether the maximum likelihood (ML) estimates of the best tree given a constrained topology differed significantly from the unconstrained best ML tree. To produce a constrained topology, *Malassezia* sequences were forced to be monophyletic, and all other branches were resolved to obtain the maximum -log likelihood using RAxML v8.2.11, with five alternative runs on distinct starting trees (-# 5) and the same amino acid model of substitution. Site-wise log-likelihood values were estimated for both trees (option: -f g in RAxML) and the resulting output was analyzed in CONSEL.

Species phylogeny. To reconstruct the phylogenetic relationship among the 14 *Malassezia* species selected, top pair-wise BLAST results of whole proteomes were clustered by a combination of the bidirectional best-hit (BDBH), COGtriangles (v2.1), and OrthoMCL (v1.4) algorithms implemented in the GET_HOMOLOGUES software package[56], to construct homologous gene families. The proteome of *M. sympodialis* ATCC42132 served as reference and clusters containing inparalogs (i.e. recent paralogs defined as sequences with best hits in its own genome) were excluded. A consensus set of 246 protein sequences was computed out of the intersection of the orthologous gene families obtained by the three clustering algorithms using the perl script *compare_clusters.pl* included in the package. These single copy orthologous gene

552 families were individually aligned with MAFFT v7.310 using the L-INS-i strategy and trimmed
553 with TrimAl (-gappyout). The resulting alignments were concatenated with the python script
554 ElConcatenero[57] to obtain a final supermatrix consisting of a total of 134,437 amino acid sites
555 (47,942 parsimony-informative). The phylogenetic tree was constructed with IQ-TREE v1.5.5
556 and the LG+F+R5 amino acid model of substitution and branch support values were obtained
557 from 10,000 replicates of both UFBoot and SH-aLRT.
558
559 **Horizontal gene transfer analyses.** To assess the extent of horizontal transfer into *Malassezia*
560 genomes, we applied a previously described pipeline [32] to the set of 15 available *Malassezia*
561 proteomes (Figure 6, Table S6), adjusting the parameters accordingly. In brief, protein sequences
562 were first aligned to the UniRef100 database (last accessed September 2017) using Diamond
563 'blastp' [58] with the following parameters: '--sensitive --index-chunks 1 --max-target-seqs 500 --
564 evalue 1e-5'. Three metrics were defined for each protein sequence used as query: (a) the HGT
565 Index [33], (b) the Alien Index (AI) [34], and (c) the Consensus Hit Support (CHS)[35]. Hits in
566 Malasseziales were omitted (NCBI taxid 162474), and we specified 'Fungi' as the ingroup
567 lineage (NCBI taxid 4751) and 'non-Fungi' as outgroup. Proteins receiving an HGT index ≥ 30,
568 AI index > 45, CHS ≥ 90, and that have Bacteria as the donor lineage, were considered well
569 supported HGT candidates and analyzed further (Figure 6 and Table S6). When a given HGT
570 candidate was detected in more than one, but not all the species, TBLASTN searches were used
571 to distinguish between *bona fide* gene losses or genome mis-annotation.
572
573 **Molecular manipulation of *M. sympodialis*.** The *M. sympodialis* flavohemoglobin-encoding
574 gene *YHB1* was identified in the genome assembly though BLASTp analysis with the
575 *Saccharomyces cerevisiae* Yhb1 protein sequence. The plasmid for targeted mutagenesis of *M.*
576 *sympodialis YHB1* was generated by cloning regions of 1.5 kb flanking the *YHB1* gene fused
577 with the *NAT* marker within the T-DNA of the binary plasmid pGI3 as previously reported[18,59].
578 For *yhb1*Δ functional complementation, three different GFP-fusion plasmids were generated.
579 The promoter (~500 bp upstream) and terminator (~200 bp downstream) of the *M. sympodialis*
580 histone H3 gene were identified in the genome assembly though BLASTp analysis with the *S.*
581 *cerevisiae* H3 as query, and amplified by PCR. The *GFP* was amplified from plasmid pSL04[60],
582 and the *NEO* marker from plasmid pAIM5[18]. The *M. sympodialis YHB1* ORF, the endogenous

M. sympodialis YHB1 gene including its native promoter and terminator, or the endogenous *M. yamatoensis YHB101* gene including its native promoter, were amplified by PCR using chimeric primers that generated recombination sites that allowed T-DNAs assembly in the following order: plasmid pGI27 was p*H3, GFP, YHB1,* t*H3, NEO*; plasmid pGI35 was p*YHB1, YHB1, GFP*, t*YHB1, NEO*, and it is referred as *YHB1-GFP*; plasmid pGI31 was p*YHB101, YHB101, GFP*, t*H3, NEO*, and it is referred as *YHB101-GFP*. For functional complementation, PCRs were performed using HF Fusion Taq according to manufacturer's instructions. Plasmids were recombined through *in vivo* recombination in *S. cerevisiae* [18]. Correct plasmids were identified by PCR and introduced into the *A. tumefaciens* EHA105 strain by electroporation, and the transformants selected on LB + 50 µg/ml kanamycin.

M. sympodialis was transformed through *Agrobacterium-tumefaciens* mediated transformation following our previously published method[19]. Transformants were selected on mDixon supplemented with nourseothricin (100 µg/ml) or neomycin G418 (100 µg/ml), and cefotaxime (350 µg/ml) to inhibit *Agrobacterium* growth. Transformants were purified to single colonies, and subjected to phenol-chloroform-isoamyl alcohol (25:24:1) DNA extraction[61]. The correct replacement of the *YHB1* target locus, as well as integration of the reconstitute versions of the *YHB1* and *YHB101* genes, were assessed by PCR. Primer sequences are listed in Table S2.

For RT-qPCR, RNA extraction was performed with the standard TRIzol method, and treated with TURBO DNAse enzyme (Thermo Fisher Scientific). The quality of the RNA was assessed using a NanoDrop spectrophotometer, and 3 µg were converted into cDNA via the Affinity Script QPCR cDNA synthesis kit (Agilent Technologies) according to manufacturer's instructions. A cDNA synthesized without the RT/RNAse block enzyme mixture was used for each sample as a control for genomic DNA contamination. Approximately 500 pg of cDNA were utilized to measure the relative expression level of target genes through quantitative real-time PCR (RT-qPCR) using the Brilliant III ultra-fast SYBR green QPCR mix (Agilent Technologies) in an Applied Biosystems 7500 Real-Time PCR System. Gene expression levels were normalized with the endogenous reference gene *TUB2* and determined using the comparative ΔΔCt method. For qualitative expression analysis, RT-qPCRs were run on agarose gel (1%), stained with ethidium bromide, and photographed under UV light.

NO quantification and GFP expression analysis. Intracellular levels of NO was measured by flow cytometry adapted from previous method[62]. In brief, *M. sympodialis* WT and *yhb1*Δ mutant were grown ON in mDixon media, washed once with PBS, and then incubated in PBS with agitation overnight. For each sample, ~ 2 x 10^8 cells/mL were equally divided, and were stained with DAF-FM DA at a final concentration of 10 µM, and the other half not stained and used as background control. Cells were washed once with PBS and analyzed using a BD FACSCantoTM II.

To measure intracellular GFP intensity by flow cytometry, *M. sympodialis yhb1*Δ mutants, and complemented strains *yhb1*Δ + *YHB1-GFP* and *yhb1*Δ + *YHB101-GFP* were grown in mDixon media ON, washed in PBS, and ~ 1 x 10^8 cells/mL used for flow cytometry analysis on the Becton-Dickinson FACScan at Duke Cancer Institute Flow Cytometry Shared Resource. The results were analyzed using FlowJo. *M. sympodialis yhb1*Δ mutants, and complemented strains *yhb1*Δ + *YHB1-GFP* and *yhb1*Δ + *YHB101-GFP* prepared in the same way were also used for GFP microscopy analysis carried out at the Duke Light Microscopy Core Facility using a Zeiss 710 inverted confocal microscope.

NO consumption assay. The NO consumption assay was performed as previously reported [63,64]. A custom□made glass reaction cell was filled with PBS (4 mL, pH 7.4, 37°C) and connected with a flow meter and a TEA NO analyzer. Under near-vacuum conditions, NO generation was achieved by injecting Deta NONOate (dissolved in 0.01□N NaOH at concentration of 30 mM) into the reaction cell. Under a helium flow, NO was passed through an inline condenser (removing water vapor) to a NO chemiluminescence analyzer (TEA 810, Ellutia) to generate an electrochemical NO baseline signal (expressed as□mV) (File S3).

We established the optimum amount of Deta NONOate as 30 µL of Deta NONOate (225 µM), leading to an increase of ~60 mV in the baseline. *Malassezia* yeasts were grown ON in mDixon, washed twice with PBS pH = 7.4, and adjusted in PBS to OD_{600}=1. Because *Malassezia* yeasts form clumps in liquid culture, cell counts using a hemocytometer was inaccurate and the number of viable cells in cultures was instead determined by plating an aliquot (100 µL) of the cellular suspensions on mDixon agar and counting colonies. The density of the *Malassezia* cultures was ~2.3 x 10^8 CFU/mL, with the exception of *M. nana* cultures that were 1.5 x 10^8 CFU/mL. For NO consumption assays the injection of a volume of PBS pH = 7.4 alone greater

than 50 µL interfered with the NO signal baseline, and therefore amounts ranging from 10 µL (2.3 x 10^6 cells injected) to 50 µL (1.15 x 10^7 cells injected) of *Malassezia* cellular suspensions were utilized. For *M. nana* injections of 15 µL (2.25 x 10^6 cells injected), 30 µL (4.50 x 10^6 cells injected) and 45 µL (6.75 x 10^6 cells injected) were performed. For technical reasons (i.e. presence of clumps, non-resuspended cells, and cultures too dense for the syringe needle) we found that the indicated range of cell counts were optimal to obtain results that were clean and reproducible.

Our standardized NO consumption assay was performed as follows: once a steady baseline was obtained (approximately 1 min), 30 µL of Deta NONOate was injected, and after a stable NO signal was achieved different volumes of *Malassezia* cellular suspensions were injected into the buffer solution (PBS + Deta NONOate), resulting in a decrease in NO signal that indicates NO consumption. Following the injection of each *Malassezia* species, the reaction chamber was flushed, and refilled with PBS and Deta NONOate. A maximum of 5 injections was performed using the same buffer solution, after which it became cloudy, generating an unstable signal.

***In vitro* phenotypic characterization of *Malassezia* strains.** Phenotypic analysis of the *Malassezia* strains reported in table S2 was performed on mDixon agar by spotting 1.5 µL of 1:10 dilutions of each cellular suspension in the following conditions: deta NONOate (0.5 mM and 1 mM), $NaNO_2$ (5 mM and 10 mM), hydrogen peroxide (1 mM), UV (200 µJ x 100), 37°C, benomyl (20 µM), 5-flucytosine (5FC, 50 and 100 µg/mL), amphotericin B (AmB, 50 µg/mL), caspofungin (2.5 µg/mL and 5 µg/mL), FLC (0.5 µg/mL and 1 µg/mL), NaCl (1M), LiCl (100 mM), Congo red (0.4 µg/mL), pH = 7.5, or pH = 4.

RNAseq analysis. 10 mL liquid mDixon cultures of ~ 1x10^7 cells/mL of *M. sympodialis* WT ATCC42132 with and without 10 mM NaNO2, and *M. sympodialis yhb1*Δ mutant were grown for ON on shaking culture at 30°C. Cells were pelleted at 3,000 rpm in a table top centrifuge for 3 minutes, washed with 10 mL dH2O, and the cell pellet was lyophilized and stored at -80°C until RNA extraction. Cells pellets was broken with sterile beads and RNA extracted with TRIzol (ThermoFisher) according to the manufacturer's instructions. Final RNA pellets were treated with TURBO DNase (ThermoFisher, catalog # AM2238) according to manufacturer's

instructions, and RNA was resuspended in 50 µl of nuclease free water. Illumina 50 bp single end libraries were prepared using the TruSeq Stranded Total RNA-seq Kit and subjected to Illumina sequencing. Library preparation and RNA sequencing was performed at the Duke University Center for Genomic and Computation Biology. Three biological replicates were performed for each sample.

After sequencing, Illumina raw reads were trimmed with Trimmomatic to remove Illumina adaptors[65] and mapped to the most recent *M. sympodialis* reference genome[66] using HiSat. Generated .bam files were used to run StringTie with the *M. sympodialis* annotation as guide, and the –e option to provide the correct output for the statistical analysis[67]. Read count information for statistical analysis were extracted using a provided python script (prepDE.py). DESeq2 was used to determine the differentially expressed genes (DEGs) as having FDR < 0.05 and $\log_2$FC ± 0.5. StringTie and DEseq2 were run on Galaxy[68]. Functional annotation of the DEGs was performed using the Blast2GO pipeline, which includes the BLASTx against the NCBI non-redundant protein database, gene ontology (GO) annotation and InterProScan[69]. Venn diagram to identify DEGs in common between the two comparisons were generated using the following web server (http://bioinformatics.psb.ugent.be/webtools/Venn/).

Flavohemoglobin purification and crystal structure. The pET28a construct expressing His-Tev-*YHB101* 2-395 (nomenclature relative to SSGCID subfeature MayaA.00765.a) was generated via Gibson assembly as follows. Overlap PCR was used to generate the final PCR product (1305 bp), which was generated from two smaller PCR products: the first PCR product (110 bp) was generated using 20 ng of an unrelated gene as template (amplifying the N-term 8XHis-Tev tag) with primers CID101552_PCR1_For and CID101552_PCR1_Rev, which add a 26 bp 5′ Gibson overlap (homologous with the NcoI-cut end of pET28a) and a 26 bp 3′ overlap with the 5′ end of the second PCR product. The second PCR product (1221 bp) was generated by PCR using 20 ng *M. yamatoensis* DNA as template (amplifying the *YHB101* coding region) with primers CID101552_PCR2_For and CID101552_PCR2_Rev, which add two stop codons and a 30 bp Gibson overlap (homologous with the HindIII-cut end of pET28a) at the 3′ end. The two PCR products were gel-purified on a 1% agarose gel (in 1X TBE + 1X Sybr Green) and 20 ng of each purified PCR was combined and used as template to generate the final PCR using outer flanking primers (CID101552_PCR1_For and CID101552_PCR2_Rev). All PCRs

were performed on an ABI Geneamp 9700 using KOD polymerase in the following conditions: initialization at 94°C for 5 min, followed by 28 cycles of denaturation at 94°C for 30 sec, annealing at 65°C for 1 min and extension at 72°C for 1.5 min, followed by a final extension step at 72°C for 7 min.

The resulting amplicon (CID101552_Final) was cloned into the NcoI/HindIII-digested pET28a via Gibson assembly according to manufacturers' instructions, and transformed into *Escherichia coli* TOP10 cells with YT + 50 µg/ml kanamycin for selection. One clone that contained no sequence errors was identified, and the DNA was used to transform *E. coli* BL21(DE3) cells, which served as starting material for expression studies.

Culture of transformed *E. coli* BL21(DE3) was transferred to 2 L of terrific broth containing 50 µg/mL and grown to OD_{600} = 0.6. Protein expression was induced by adding 1 mM Isopropyl β-D-1-thiogalactopyranoside (IPTG) and grown for 45 hours at 25°C. 5-aminoluevulinic acid 0.3 mM was added at the time of induction to facilitate heme biosynthesis. The cells were harvested by centrifugation and the pellets stored at –80°C. Cells were resuspended at 1g:5mL ratios in 25 mM Tris-HCl pH = 8.0 (Teknova), 200 mM NaCl (Teknova), 0.5% 3-[(3-Cholamidopropyl)dimethylammonio]-1-propanesulfonate (CHAPS) (JT Baker), 50 mM L-arginine (Sigma), 500 U of benzonase (Novagen), 100 mg lysozyme (Sigma) and one EDTA free protease inhibitor tablet (Roche). The cells were lysed via microfluidization (Microfluidics) with two passes at 15,000 PSI on ice and clarified via centrifugation at 200 rcf for 45 minutes at 4°C, and filtered with a 0.2 µm PES bottle top filter (Nalgene). The supernatant was applied to four 5 mL Ni^{2+} charged HiTrap Chelating HP (GE Healthcare) columns and the protein eluted with a 500 mM imidazole gradient over 15 column volumes. The fractions of interest (which were visibly red-brown) were pooled and the His-TEV tag was removed via cleavage with His-tagged Tobacco etch virus protease 1 (TEV, produced in-house) while dialyzing against 2 L of 25 mM Tris pH = 8.0 and 200 mM NaCl overnight at 4°C using 10 kDa MWCO snakeskin dialysis tubing (Thermo scientific/Pierce). The affinity tag was removed by applying the digested pool over one 5 mL Ni2+ charged HiTrap Chelating HP columns. The cleaved protein bound and eluted from the column before the remaining uncleaved material and separate pools were made for both. The protein pools were concentrated for size exclusion chromatography via centrifugal concentration (Vivaspin Polyethylsulfone, 10 kDa MWCO, Sartorius) to 3.81 mg/mL (cleaved pool) and 14.5 mg/ml (uncleaved pool) for

injection over a Superdex75 (GE Healthcare) in 10 mM HEPES (2-[4-(2-hydroxyethyl)piperazin-1-yl]ethanesulfonic acid), pH 7.5 and 150 mM NaCl. Fractions of interest were pooled and concentrated via centrifugal concentration (Vivaspin Polyethylsulfone, 10kDa MWCO, Sartorius) to 5.74 mg/mL (cleaved pool) and 19.93 mg/mL (uncleaved pool), aliquoted and stored at –80°C.

Apo *M. yamatoensis* flavohemoglobin protein (SSGCID ID MayaA.00765.a.TH11.PD38344, uncleaved pool) was set up for crystallization as sitting drops in 96-well XJR trays (Rigaku Reagents) with 0.4 ul reservoir solution and 0.4 ul protein at 19.93 mg/ml. Trays were then stored at 14°C. Crystallization conditions were searched for using commercial sparse matrix screens JCSG+, JCSG-Top96, Wizard 3/4 (Rigaku Reagents), MCSG-1 (Microlytic), and Morpheus (Molecular Dimensions). Crystals were obtained with Morpheus B12: 12.5% (w/v) PEG1000, 12.5% (w/v) PEG3350, 12.5% (v/v) MPD, 0.03 M each sodium fluoride, sodium bromide, and sodium iodide, and 0.1 M bicine/Trizma base pH 8.5. After 35 days, red-brown crystals were harvested directly from the droplet, frozen in liquid nitrogen, and stored for screening.

Data were collected on a Rigaku FR-E+ 007 SuperBright rotating anode equipped with Rigaku Varimax optics and a Saturn 944+ detector. The data set was processed with the XDS package[70]. Friedel pairs were kept separate for the calculation of anomalous maps. Initial phases were calculated with Phaser EP[71] within the CCP4 package[72] and the CCP4 program PARROT[73] was used for phase improvement. An initial model was built with ARPwARP[74]. The structure was refined with phenix.refine[75] within Phenix[76] and manual model building was done using Coot[77]. Built-in tools in Coot were used to assess structure quality before each refinement. Ligand restraints for bound heme and FAD were generated using Grade web server (http://grade.globalphasing.org) from GlobalPhasing Ltd. Model quality was validated using MolProbity[78]. The final structure factors and coordinates were deposited in the PDB[79,80] with code 6O0A. Structural images were generated using Chimera software[81]. The flavohemoglobin structures of *E. coli* (PDB ID 1GVH) and *Saccharomyces cerevisiae* (PDB ID 4G1V) were used for comparison with that of *M. yamatoensis.*

Interaction of *M. sympodialis* strains with the host. The ability of *M. sympodialis* WT, *yhb1*Δ mutant, and complemented strains *yhb1*Δ + *YHB1-GFP* and *yhb1*Δ + *YHB101-GFP* to survive

within macrophage was carried out according to previous protocol[28,82]. J774 A.1 cells (1 × 10^5/well) were added to 96-well plates and activated by addition of either 1) 10 nM phorbol myristate acetate (PMA) and incubated for 1 h at 37 °C with 5% CO_2, 2) 100 U/mL interferon-γ and LPS (0.6 µg/mL) and incubated overnight at 37˚C 5% CO_2. Two days old cultures of *M. sympodialis* were washed twice with sterile water, and resuspended in RPMI + human serum 20 % for opsonization for 2 h at 37˚C. *M. sympodialis* cells were washed three times with water, resuspended in DMEM and added to the macrophages at a 1:1 yeasts: macrophages ratio. Plates were incubated for 2 h at 37 °C in 5% CO2, then the co-cultures were washed three times with PBS to remove yeasts that were not internalized, and the plate was incubated at 37 °C in 5% CO2 for 18 h. Yeast cells were collected by lysing macrophages, and from each condition a 1:20 dilution was plated on mDixon agar and incubated at 30 °C for 3-5 days to determine yeast survival.

For *in vivo* infection experiments, WT C57BL/6j mice were purchased from Janvier Elevage. *Nos2*-/- mice [83] were obtained from Nicolas Fasel (Lausanne). Mice were maintained at the Laboratory Animal Science Center of University of Zurich, Zurich, Switzerland and used at 6-12 weeks in sex- and age-matched groups. Epicutaneous infection of the mouse ear skin was performed as described previously [5,84].Briefly, *Malassezia* strains were grown for 3-4 days at 30°C, 180 rpm in liquid mDixon medium. Cells were washed in PBS and suspended in native olive oil at a density of 20 OD_{A600}/mL. 100 µl suspension (corresponding to 2 OD_{A600}) of yeast cells was applied topically onto the dorsal ear skin that was previously barrier-disrupted by mild tape stripping while mice were anaesthetized. For determining the fungal loads in the skin, tissue was transferred in water supplemented with 0.05% Nonidet P40 (AxonLab), homogenized and plated on modified Dixon agar and incubated at 30°C for 3-4 days. For quantification of cellular infiltrates, single cell suspensions of ear skin were stained with antibodies directed against CD45 (clone 104), CD11b (clone M1/70), Ly6G (clone 1A8), Ly6C (clone HK1.4) in PBS supplemented with 1% FCS, 5 mM EDTA and 0.02% NaN_3. LIVE/DEAD Near IR stain (Life Technologies) was used for exclusion of dead cells. Cells were acquired on a FACS Cytoflex (Beckman Coulter) and the data were analyzed with FlowJo software (FlowJo LLC). The gating of the flow cytometric data was performed according to the guidelines for the use of flow cytometry and cell sorting in immunological studies [85], including pre-gating on viable and single cells for analysis. For transcript expression analysis, total RNA was isolated from ear skin

according to standard protocols using TRI Reagent (Sigma Aldrich). cDNA was generated by RevertAid reverse transcriptase (Thermo Fisher). Quantitative PCR was performed using SYBR Green (Roche) and a QuantStudio 7 Flex (Life Technologies) instrument. The primers used for qPCR were as follows: *Il17a* forward 5'-GCTCCAGAAGGCCCTCAGA-3', reverse 5'-AGCTTTCCCTCCGCATTGA-3' [86]; *Defb3* forward 5- GTCTCCACCTGCAGCTTTTAG-3', reverse 5'- ACTGCCAATCTGACGAGTGTT-3' [87]; *Nos2* forward 5'-GTTCTCAGCCCAACAATACAAGA-3', reverse 5'- GTGGACGGGTCGATGTCAC-3'; *Actb* forward 5--CCCTGAAGTACCCCATTGAAC-3', reverse 5'-CTTTTCACGGTTGGCCTTAG-3'. All RT-qPCR assays were performed in duplicates and the relative expression (rel. expr.) of each gene was determined after normalization to *Actb* transcript levels.

ACKNOWLEDGMENTS

We thank Stephen Rogers for assistance with the NO consumption assay, Nicolas Fasel for *Nos2*-/- mice, Ellen Wallace for her contribution to cloning the *Malassezia* crystallography constructs, Jan Abendroth for his contributions to solving the structure of *Malassezia* by phasing off the bound iron, Jason Yano and Rana Sidhu for consultation on improving heme incorporation during recombinant expression of the crystallography constructs, and Tom Edwards and Don Lorimer for their overall support of the project.

FUNDING INFORMATION

This work was in part supported by NIH/NIAID R01 grant AI50113-15, and by NIH/NIAID R37 MERIT award AI39115-21 (to J.H.) and by SNF grant 310030_189255 (to S.L.L.). VA Merit BX-003478 supported TJM's work. Crystallization work was funded by the NIH/NIAD (contract nos. HHSN272200700057, HHSN272201200025C, and HHSN272201700059C to Peter J. Myler). Joseph Heitman is Co-Director and Fellow of the CIFAR program "Fungal Kingdom: Threats and Opportunities".

Figures

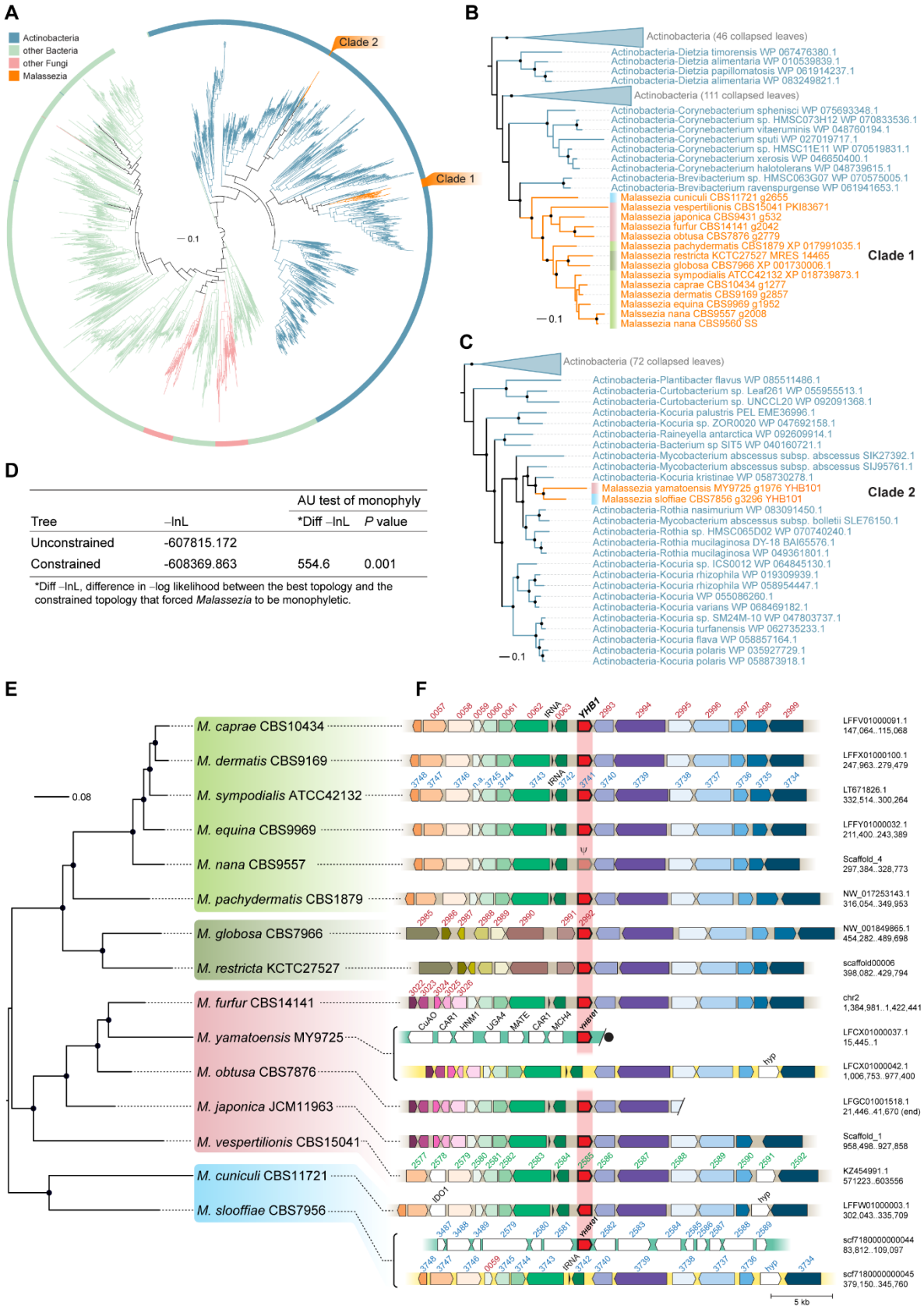

845

Tree	−lnL	AU test of monophyly *Diff −lnL	*P* value
Unconstrained	-607815.172		
Constrained	-608369.863	554.6	0.001

*Diff −lnL, difference in −log likelihood between the best topology and the constrained topology that forced *Malassezia* to be monophyletic.

Figure 1. Evidence for two independent HGT events of the flavohemoglobin-encoding genes in *Malassezia* from the Actinobacteria. (A) Maximum likelihood phylogeny of consisting of 2,155 flavohemoglobin protein sequences. Two groups (clade 1 and 2) of horizontally transferred flavohemoglobin genes (*YHB1* and *YHB101*) in *Malassezia* are colored orange. Other tree branches are colored according to the key on the top left, representing other major groups of organisms. The phylogeny was visualized using iTOL v3.6.1[88] and was rooted at the midpoint. (B - C) Zoomed views of the ML phylogeny showing in more detail the position of *Malassezia* flavohemoglobins from clades 1 and 2, and their putative bacterial donor lineages. (D) Results of topological constraints tests that significantly rejected the monophyletic origin for both *Malassezia* flavohemoglobins clades, providing additional support for independent HGT events. (E) Phylogenetic relationship of *Malassezia* species with available genome data inferred from the concatenation of 246 single-copy proteins. Color codes assigned to the different, highly supported, phylogenetic clades are kept consistent in all figures. The tree was rooted at the midpoint and branch support values are given as shown in the key. (F) Chromosomal regions encompassing the *YHB1* gene in *Malassezia*. Genes are shown as arrows denoting the direction of transcription and orthologs are represented in the same color. Non-syntenic genes are shown in white, and small arrows in black represent tRNAs. The *YHB1* gene is shown as red arrows outlined in bold in the center. The end of a scaffold is represented by a forward slash. For *M. yamatoensis* and *M. slooffiae*, yellow bars indicate the absence of the *YHB1* gene in otherwise syntenic regions, and those in green indicate instances where another flavohemoglobin-encoding gene (named *YHB101*) was acquired by an independent HGT event. A possibly defective *YHB1* gene in *M. nana* CBS9557 is denoted by the Greek symbol ψ. Gene codes in red or blue are as they appear in *M. globosa* (prefix "MGL_") or *M. sympodialis* (prefix "MSYG_") genome annotations, respectively, those in black were named based on top BLASTp hits in *S. cerevisiae*, and "hyp" represent hypothetical proteins. Black circle represents the end of a chromosome; scaffold/chromosomal locations and accession numbers are given for each region.

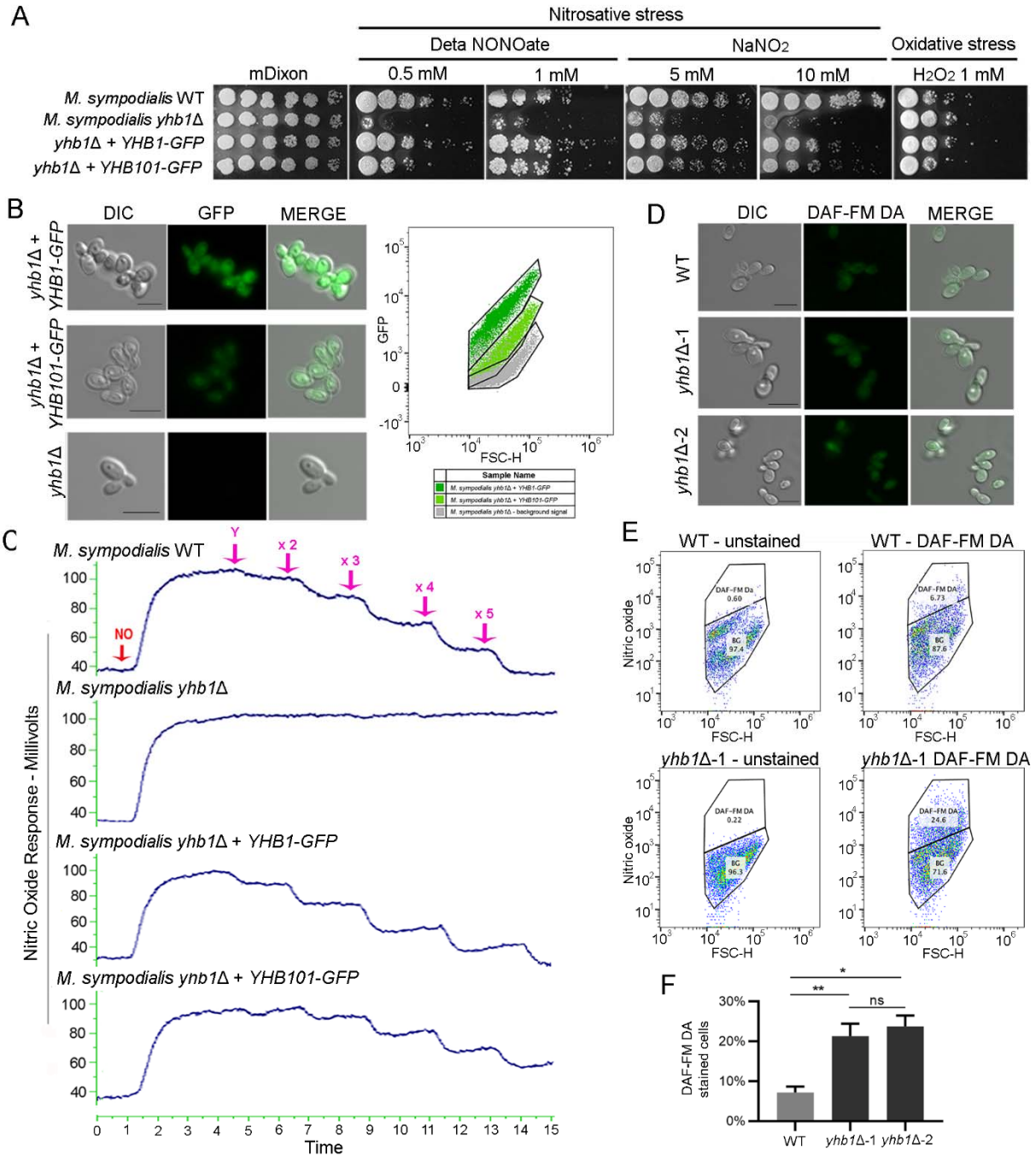

Figure 2. *M. sympodialis* flavohemoglobins are involved in nitrosative stress resistance and NO degradation. (A) Stress sensitivity assay of *M. sympodialis* WT, *yhb1*Δ mutant, and complementing strains *yhb1*Δ + *YHB1* and *yhb1*Δ + *YHB101* on mDixon agar supplemented with the NO-donor agent Deta NONOate and $NaNO_2$, and with hydrogen peroxide. (B) GFP expression in the *M. sympodialis yhb1*Δ mutant, and complementing strains *yhb1*Δ + *YHB1* and

*yhb1*Δ + *YHB101*, and respective GFP signal analyzed trough FACS. (C) NO consumption assay by *M. sympodialis* WT, *yhb1*Δ mutant, and complementing strains *M. sympodialis* WT, *yhb1*Δ mutant, and complementing strains *yhb1*Δ + *YHB1* and *yhb1*Δ + *YHB101*; the blue trace indicates the NO level over a period of 15 min. NO and *Malassezia* (Y = yeast) injections are indicated by purple arrows. In this experiment, 10 µL (Y), 20 µL (x 2) and 30 µL (x 3), 40 µL (x 4) and 50 µL (x 5) of *Malassezia* cellular suspensions were injected. (D) Representative fluorescent staining of intracellular NO with DAF-FM DA in *M. sympodialis* WT and two independent *yhb1*Δ mutants, and (E-F) quantification of the NO signal by flow cytometry; spontaneous fluorescence of *M. sympodialis* was used as background to detect specifically DAF-FM DA signal. Asterisks indicates statistically significant differences (* = $p<0.05$, ** = $p<0.01$) according to the unpaired student's t-test with Welch's correction.

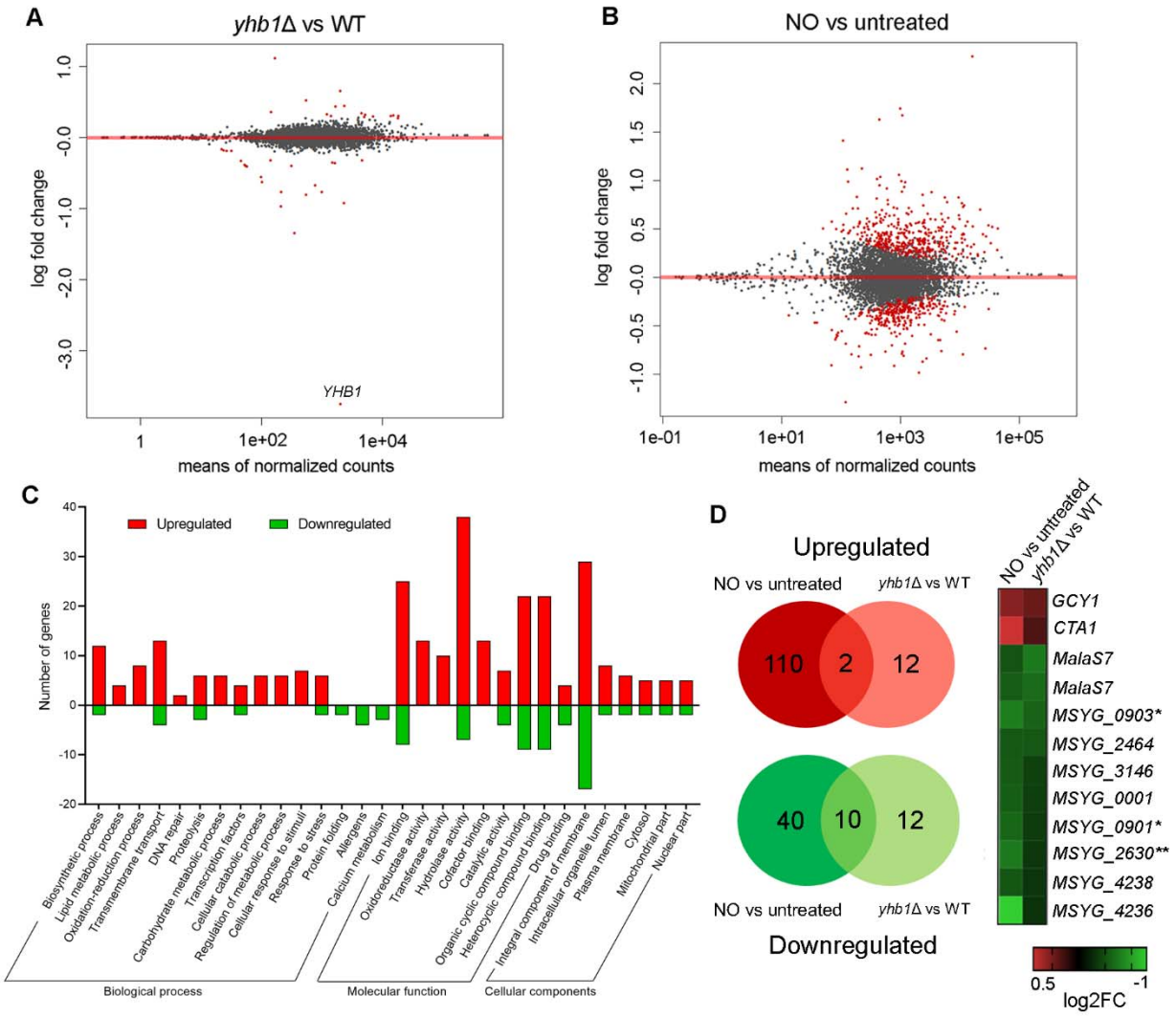

Figure 3. Transcriptomic profile of *M. sympodialis yhb1*Δ and WT strain. (A) MA-plot displaying the transcriptomic changes of the *M. sympodialis yhb1*Δ mutant compared to the WT strain. Red dots indicate differentially expressed genes for FDR < 0.05; the *YHB1* gene is indicated and its represent an internal control, its downregulation is expected because the gene is deleted. (B) MA-plot displaying the transcriptomic changes of *M. sympodialis* WT grown in the presence of the NO-donor NaNO2 compared to the untreated control. Red dots indicate differentially expressed genes for FDR < 0.05. (C) Gene ontology classification relative to the RNAseq condition reported in B. Upregulated genes are indicated in red, and downregulated genes are indicated in green. (D) Venn diagrams comparison of the upregulated and downregulated genes relative to RNAseq conditions reported in A and B; the panel on the right

shows a heatmap of the log2FC of the shared upregulated (red) and downregulated (green) genes. Predicted allergens are indicated with one asterisk, and two asterisks indicate a secreted lipase.

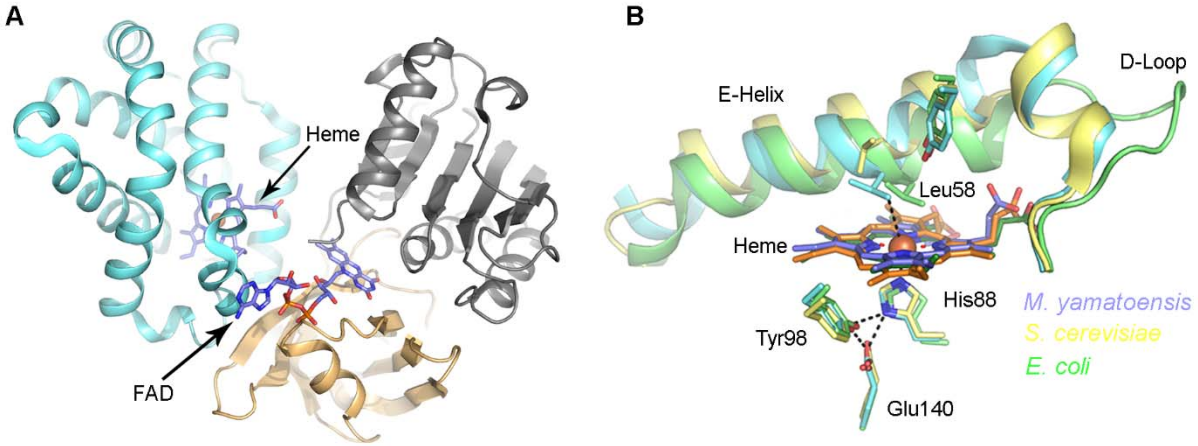

Figure 4. 3-dimensional X-ray crystal structure of the *M. yamatoensis* flavohemoglobin Yhb101. (A) The globin domain (cyan) binds a heme molecule. The reductase domain consists of an FAD-binding domain (gray) and an NAD-binding domain (tan) that bind an FAD molecule. (B) An overlay of flavohemoglobin globin domains from fungus, bacteria, and yeast. Globin domains of *M. yamatoensis* (PDB ID 6O0A; blue), *S. cerevisiae* (PDB ID 4G1V; yellow), and *E. coli* (PDB ID 1GVH; green) show structural similarity.

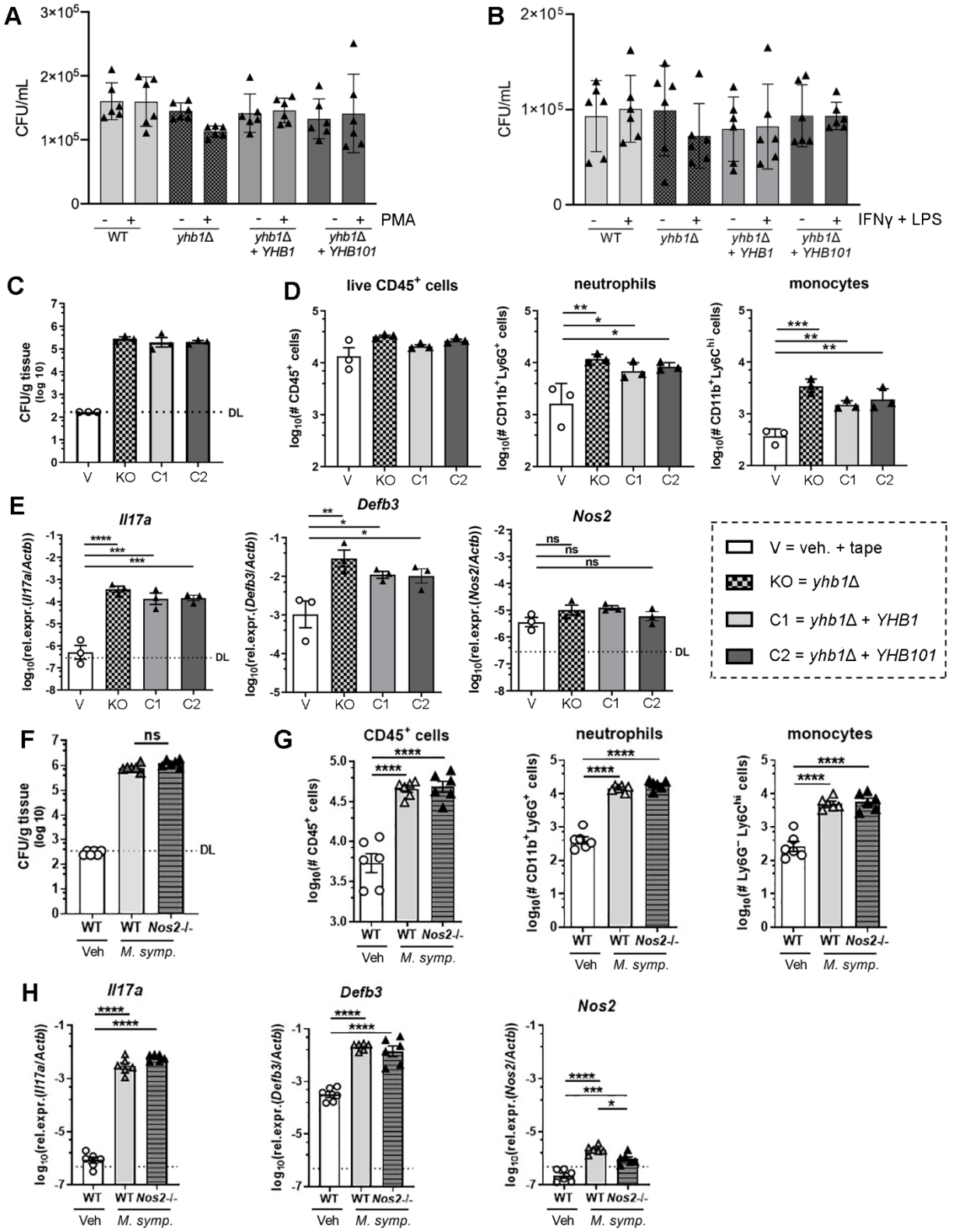
A
CFU/mL
PMA
WT
yhb1Δ
yhb1Δ + YHB1
yhb1Δ + YHB101
B
IFNγ + LPS
C
CFU/g tissue (log 10)
DL
V
KO
C1
C2
D
live CD45+ cells
neutrophils
monocytes
E
Il17a
Defb3
Nos2
V = veh. + tape
KO = yhb1Δ
C1 = yhb1Δ + YHB1
C2 = yhb1Δ + YHB101
F
ns
Veh
M. symp.
Nos2-/-
G
CD45+ cells
H

Figure 5. *Malassezia* flavohemoglobins are not required for pathogenesis in *ex vivo* and *in vivo* models. (A-B) *M. sympodialis* WT, *yhb1*Δ, *yhb1*Δ + *YHB1*, and *yhb1*Δ + *YHB101* were opsonized with 20% human serum and added to J774A.1 macrophage (1:1 ratio) activated with phorbol myristate acetate (PMA) (A) or interferon-gamma + lipopolysaccharide (IFNγ + LPS) (B). After 24 h, J774A.1 cells were lysed and *M. sympodialis* cells were harvested and plated on selective media to determine CFUs. Data are expressed as CFU/mL. (C-E) WT C57BL/6j mice were infected epicutaneously with *M. sympodialis* WT, *yhb1*Δ, *yhb1*Δ + *YHB1*, and *yhb1*Δ + *YHB101*. Skin colony forming units (CFU) (C), cellular infiltrates (D) and *Il17a*, *Defb3* and *Nos2* transripts (E) were analyzed on day 4 post infection. (F-H) WT and *Nos2*-/- mice were infected epicutaneously with *M. sympodialis* WT. Skin CFU (F), cellular infiltrates (G) and *Il17a*, *Defb3* and *Nos2* transcripts (H) were analyzed on day 5 post infection. Graphs show the mean + SEM of each group. Individual samples are also indicated with each symbol representing one well (A-B) or one mouse (C-H). The dotted line indicates the detection limit. Data are from one experiment (C-E) or pooled from two independent experiments (A-B, F-H). Statistics are calculated using one-way ANOVA with Sidak's multiple comparisons test. *$p<0.05$, **$p<0.01$, ***$p<0.001$, ****$p<0.0001$.

Figure 6. *Malassezia* genes acquired through HGT from bacteria. HGT candidates identified in the genomes of the 15 *Malassezia* species (represented on the top according to their phylogenetic classification) are shown as different lines in the presence-absence matrix, with the closest ortholog in *S. cerevisiae* indicated in parenthesis, where available. For each HGT candidate, the presence of the gene in a genome is indicated by orange square, and the intensity of the color is correlated with the gene copy number (numbers in white). HGT candidates occurring in multiple *Malassezia* species are shown in the top half of the matrix, whereas those that are species-specific HGT candidates are shown in the bottom half of the matrix, and color-coded as shown in the key. Asterisks indicate HGT candidate genes identified in the previous study [3].

Supplemental table legends

Table S1. Upregulated differentially expressed genes for FDR <0.05 in the condition *M. sympodialis yhb1*Δ versus *M. sympodialis* WT. Highlighted in yellows are DEGs with $\log_2$FC < 0.5.

Table S2. Downregulated differentially expressed genes for FDR <0.05 in the condition *M. sympodialis yhb1*Δ versus *M. sympodialis* WT. Highlighted in yellows are DEGs with $\log_2$FC < -0.5.

Table S3. Upregulated differentially expressed genes for FDR <0.05 and $\log_2$FC + 0.05 in the condition *M. sympodialis* WT + $NaNO_2$ versus *M. sympodialis* WT untreated.

Table S4. Downregulated differentially expressed genes for FDR <0.05 and $\log_2$FC - 0.05 in the condition *M. sympodialis* WT + $NaNO_2$ versus *M. sympodialis* WT untreated.

Table S5. Data collection, phasing and refinement statistics relative to the X-ray structure of *M. yamatoensis* flavohemoglobin.

Table S6. Summary of the HGT candidate genes identified in *Malassezia* species. Each sheet is indicated with a color that matches *Malassezia* phylogeny represented in Figures 1E and 6.

References

1 Findley, K. *et al.* Topographic diversity of fungal and bacterial communities in human skin. *Nature* **498**, 367-370, doi:10.1038/nature12171 (2013).

2 Theelen, B. *et al.* *Malassezia* ecology, pathophysiology, and treatment. *Medical Mycology* **56**, S10-S25, doi:10.1093/mmy/myx134 (2018).

3 Wu, G. *et al.* Genus-wide comparative genomics of *Malassezia* delineates its phylogeny, physiology, and niche adaptation on human skin. *PLOS Genetics* **11**, e1005614, doi:10.1371/journal.pgen.1005614 (2015).

4 Gaitanis, G., Magiatis, P., Hantschke, M., Bassukas, I. D. & Velegraki, A. The *Malassezia* genus in skin and systemic diseases. *Clin Microbiol Rev* **25**, 106-141, doi:10.1128/cmr.00021-11 (2012).

5 Sparber, F. *et al.* The skin commensal yeast *Malassezia* triggers a type 17 response that coordinates anti-fungal immunity and exacerbates skin inflammation. *Cell Host & Microbe* **25**, 389-403.e386, doi:10.1016/j.chom.2019.02.002 (2019).

6 Limon, J. J. *et al.* *Malassezia* is associated with Crohn's disease and exacerbates colitis in mouse models. *Cell Host & Microbe* **25**, 377-388.e376, doi:10.1016/j.chom.2019.01.007 (2019).

7 Aykut, B. *et al.* The fungal mycobiome promotes pancreatic oncogenesis via activation of MBL. *Nature* **574**, 264-267, doi:10.1038/s41586-019-1608-2 (2019).

8 Astuti, R. I., Nasuno, R. & Takagi, H. Nitric oxide signaling in yeast. *Appl Microbiol Biotechnol* **100**, 9483-9497, doi:10.1007/s00253-016-7827-7 (2016).

9 Forrester, M. T. & Foster, M. W. Protection from nitrosative stress: a central role for microbial flavohemoglobin. *Free radical biology & medicine* **52**, 1620-1633, doi:10.1016/j.freeradbiomed.2012.01.028 (2012).

10 Gupta, S., Pawaria, S., Lu, C., Yeh, S. R. & Dikshit, K. L. Novel flavohemoglobins of mycobacteria. *IUBMB life* **63**, 337-345, doi:10.1002/iub.460 (2011).

11 Thakur, N., Kumar, A. & Dikshit, K. L. Type II flavohemoglobin of Mycobacterium smegmatis oxidizes d-lactate and mediate electron transfer. *International Journal of Biological Macromolecules* **112**, 868-875, doi:https://doi.org/10.1016/j.ijbiomac.2018.02.010 (2018).

12 Hoogewijs, D., Dewilde, S., Vierstraete, A., Moens, L. & Vinogradov, S. N. A phylogenetic analysis of the globins in fungi. *PLoS One* **7**, e31856, doi:10.1371/journal.pone.0031856 (2012).

13 Wisecaver, J. H., Alexander, W. G., King, S. B., Hittinger, C. T. & Rokas, A. Dynamic evolution of nitric oxide detoxifying flavohemoglobins, a family of single-protein metabolic modules in bacteria and eukaryotes. *Mol Biol Evol* **33**, 1979-1987, doi:10.1093/molbev/msw073 (2016).

14 Vinogradov, S. N. *et al.* A phylogenomic profile of globins. *BMC Evolutionary Biology* **6**, 31, doi:10.1186/1471-2148-6-31 (2006).

15 Liu, L., Zeng, M., Hausladen, A., Heitman, J. & Stamler, J. S. Protection from nitrosative stress by yeast flavohemoglobin. *Proc Natl Acad Sci U S A* **97**, 4672-4676, doi:10.1073/pnas.090083597 (2000).

16 Husnik, F. & McCutcheon, J. P. Functional horizontal gene transfer from bacteria to eukaryotes. *Nature reviews. Microbiology* **16**, 67-79, doi:10.1038/nrmicro.2017.137 (2018).

17 Ropars, J. *et al.* Adaptive horizontal gene transfers between multiple cheese-associated fungi. *Curr Biol* **25**, 2562-2569, doi:10.1016/j.cub.2015.08.025 (2015).
18 Ianiri, G., Averette, A. F., Kingsbury, J. M., Heitman, J. & Idnurm, A. Gene function analysis in the ubiquitous human commensal and pathogen *Malassezia* genus. *mBio* **7**, e01853-01816, doi:10.1128/mBio.01853-16 (2016).
19 Ianiri, G., Applen Clancey, S., Lee, S. C. & Heitman, J. FKBP12-dependent inhibition of calcineurin mediates immunosuppressive antifungal drug action in *Malassezia*. *mBio* **8**, e01752-01717, doi:10.1128/mBio.01752-17 (2017).
20 Wang, X. *et al.* Biological activity of nitric oxide in the plasmatic compartment. *Proc Natl Acad Sci U S A* **101**, 11477-11482, doi:10.1073/pnas.0402201101 (2004).
21 Nakano, M. M. Essential role of flavohemoglobin in long-term anaerobic survival of *Bacillus subtilis*. *Journal of bacteriology* **188**, 6415-6418, doi:10.1128/jb.00557-06 (2006).
22 Hirai, A. *et al. Malassezia nana* sp. nov., a novel lipid-dependent yeast species isolated from animals. *Int J Syst Evol Microbiol* **54**, 623-627, doi:10.1099/ijs.0.02776-0 (2004).
23 Horan, S., Bourges, I. & Meunier, B. Transcriptional response to nitrosative stress in *Saccharomyces cerevisiae*. *Yeast* **23**, 519-535, doi:10.1002/yea.1372 (2006).
24 Yang, D.-H. *et al.* Rewiring of signaling networks modulating thermotolerance in the human pathogen *Cryptococcus neoformans*. *Genetics* **205**, 201-219, doi:10.1534/genetics.116.190595 (2017).
25 Veri, A. O. *et al.* Tuning Hsf1 levels drives distinct fungal morphogenetic programs with depletion impairing Hsp90 function and overexpression expanding the target space. *PLOS Genetics* **14**, e1007270, doi:10.1371/journal.pgen.1007270 (2018).
26 El Hammi, E. *et al.* Active site analysis of yeast flavohemoglobin based on its structure with a small ligand or econazole. *FEBS J* **279**, 4565-4575, doi:10.1111/febs.12043 (2012).
27 Ilari, A., Bonamore, A., Farina, A., Johnson, K. A. & Boffi, A. The X-ray structure of ferric *Escherichia coli* flavohemoglobin reveals an unexpected geometry of the distal heme pocket. *J Biol Chem* **277**, 23725-23732, doi:10.1074/jbc.M202228200 (2002).
28 de Jesus-Berrios, M. *et al.* Enzymes that counteract nitrosative stress promote fungal virulence. *Curr Biol* **13**, 1963-1968 (2003).
29 Hromatka, B. S., Noble, S. M. & Johnson, A. D. Transcriptional response of *Candida albicans* to nitric oxide and the role of the *YHB1* gene in nitrosative stress and virulence. *Mol Biol Cell* **16**, 4814-4826, doi:10.1091/mbc.e05-05-0435 (2005).
30 Lapp, K. *et al.* Characterization of the *Aspergillus fumigatus* detoxification systems for reactive nitrogen intermediates and their impact on virulence. *Frontiers in microbiology* **5**, 469-469, doi:10.3389/fmicb.2014.00469 (2014).
31 Winter, S. E. *et al.* Host-derived nitrate boosts growth of *E. coli* in the inflamed gut. *Science* **339**, 708-711, doi:10.1126/science.1232467 (2013).
32 Nowell, R. W. *et al.* Comparative genomics of bdelloid rotifers: Insights from desiccating and nondesiccating species. *PLOS Biology* **16**, e2004830, doi:10.1371/journal.pbio.2004830 (2018).
33 Boschetti, C. *et al.* Biochemical diversification through foreign gene expression in bdelloid rotifers. *PLOS Genetics* **8**, e1003035, doi:10.1371/journal.pgen.1003035 (2012).
34 Alexander, W. G., Wisecaver, J. H., Rokas, A. & Hittinger, C. T. Horizontally acquired genes in early-diverging pathogenic fungi enable the use of host nucleosides and

nucleotides. *Proceedings of the National Academy of Sciences* **113**, 4116-4121, doi:10.1073/pnas.1517242113 (2016).

35 Koutsovoulos, G. *et al.* No evidence for extensive horizontal gene transfer in the genome of the tardigrade *Hypsibius dujardini*. *Proceedings of the National Academy of Sciences* **113**, 5053-5058, doi:10.1073/pnas.1600338113 (2016).

36 Beceiro, A., Tomás, M. & Bou, G. Antimicrobial resistance and virulence: a successful or deleterious association in the bacterial world? *Clinical Microbiology Reviews* **26**, 185-230, doi:10.1128/cmr.00059-12 (2013).

37 Mosqueda, N. *et al.* Characterization of plasmids carrying the blaOXA-24/40 carbapenemase gene and the genes encoding the AbkA/AbkB proteins of a toxin/antitoxin system. *The Journal of antimicrobial chemotherapy* **69**, 2629-2633, doi:10.1093/jac/dku179 (2014).

38 Tkach, J. M. *et al.* Dissecting DNA damage response pathways by analysing protein localization and abundance changes during DNA replication stress. *Nat Cell Biol* **14**, 966-976, doi:10.1038/ncb2549 (2012).

39 Rep, M. *et al.* The *Saccharomyces cerevisiae* Sko1p transcription factor mediates HOG pathway-dependent osmotic regulation of a set of genes encoding enzymes implicated in protection from oxidative damage. *Mol Microbiol* **40**, 1067-1083 (2001).

40 Lacroix, B. & Citovsky, V. Transfer of DNA from bacteria to eukaryotes. *mBio* **7**, e00863-00816, doi:10.1128/mBio.00863-16 (2016).

41 Murphy, C. L. *et al.* Horizontal gene transfer as an indispensable driver for Neocallimastigomycota evolution into a distinct gut-dwelling fungal lineage. *Applied and environmental microbiology*, AEM.00988-00919, doi:10.1128/aem.00988-19 (2019).

42 Cals-Grierson, M. M. & Ormerod, A. D. Nitric oxide function in the skin. *Nitric oxide : biology and chemistry* **10**, 179-193, doi:10.1016/j.niox.2004.04.005 (2004).

43 Nittler, M. P., Hocking-Murray, D., Foo, C. K. & Sil, A. Identification of *Histoplasma capsulatum* transcripts induced in response to reactive nitrogen species. *Molecular biology of the cell* **16**, 4792-4813, doi:10.1091/mbc.e05-05-0434 (2005).

44 Amend, A. From Dandruff to Deep-Sea Vents: *Malassezia*-like fungi are ecologically hyper-diverse. *PLoS pathogens* **10**, e1004277, doi:10.1371/journal.ppat.1004277 (2014).

45 Stanke, M. & Morgenstern, B. AUGUSTUS: a web server for gene prediction in eukaryotes that allows user-defined constraints. *Nucleic Acids Res* **33**, W465-467, doi:10.1093/nar/gki458 (2005).

46 Jones, P. *et al.* InterProScan 5: genome-scale protein function classification. *Bioinformatics (Oxford, England)* **30**, 1236-1240, doi:10.1093/bioinformatics/btu031 (2014).

47 Fu, L., Niu, B., Zhu, Z., Wu, S. & Li, W. CD-HIT: accelerated for clustering the next-generation sequencing data. *Bioinformatics (Oxford, England)* **28**, 3150-3152, doi:10.1093/bioinformatics/bts565 (2012).

48 Katoh, K. & Standley, D. M. MAFFT multiple sequence alignment software version 7: improvements in performance and usability. *Mol Biol Evol* **30**, 772-780, doi:10.1093/molbev/mst010 (2013).

49 Capella-Gutierrez, S., Silla-Martinez, J. M. & Gabaldon, T. trimAl: a tool for automated alignment trimming in large-scale phylogenetic analyses. *Bioinformatics* **25**, 1972-1973, doi:10.1093/bioinformatics/btp348 (2009).

50 Nguyen, L. T., Schmidt, H. A., von Haeseler, A. & Minh, B. Q. IQ-TREE: a fast and effective stochastic algorithm for estimating maximum-likelihood phylogenies. *Mol Biol Evol* **32**, 268-274, doi:10.1093/molbev/msu300 (2015).

51 Kalyaanamoorthy, S., Minh, B. Q., Wong, T. K. F., von Haeseler, A. & Jermiin, L. S. ModelFinder: fast model selection for accurate phylogenetic estimates. *Nature methods* **14**, 587-589, doi:10.1038/nmeth.4285 (2017).

52 Minh, B. Q., Nguyen, M. A. & von Haeseler, A. Ultrafast approximation for phylogenetic bootstrap. *Mol Biol Evol* **30**, 1188-1195, doi:10.1093/molbev/mst024 (2013).

53 Guindon, S. *et al.* New algorithms and methods to estimate maximum-likelihood phylogenies: assessing the performance of PhyML 3.0. *Systematic Biology* **59**, 307-321, doi:10.1093/sysbio/syq010 (2010).

54 Shimodaira, H. & Hasegawa, M. CONSEL: for assessing the confidence of phylogenetic tree selection. *Bioinformatics* **17**, 1246-1247 (2001).

55 Shimodaira, H. An approximately unbiased test of phylogenetic tree selection. *Syst Biol* **51**, 492-508, doi:10.1080/10635150290069913 (2002).

56 Contreras-Moreira, B. & Vinuesa, P. GET_HOMOLOGUES, a versatile software package for scalable and robust microbial pangenome analysis. *Appl Environ Microbiol* **79**, 7696-7701, doi:10.1128/aem.02411-13 (2013).

57 ODiogoSilva. ElConcatenero (Version v1.0). *Zenodo.* , doi:http://doi.org/10.5281/zenodo.10588 (2014).

58 Buchfink, B., Xie, C. & Huson, D. H. Fast and sensitive protein alignment using DIAMOND. *Nature methods* **12**, 59-60, doi:10.1038/nmeth.3176 (2015).

59 Ianiri, G., Boyce, K. J. & Idnurm, A. Isolation of conditional mutations in genes essential for viability of *Cryptococcus neoformans*. *Curr Genet* **63**, 519-530, doi:10.1007/s00294-016-0659-2 (2017).

60 Lee, S. C. & Heitman, J. Function of *Cryptococcus neoformans KAR7* (*SEC66*) in karyogamy during unisexual and opposite-sex mating. *Eukaryot Cell* **11**, 783-794, doi:10.1128/ec.00066-12 (2012).

61 Hoffman, C. S. in *Current Protocols in Molecular Biology* (John Wiley & Sons, Inc., 2001).

62 Koch, B. *et al.* A metabolic checkpoint for the yeast-to-hyphae developmental switch regulated by endogenous nitric oxide signaling. *Cell reports* **25**, 2244-2258.e2247, doi:https://doi.org/10.1016/j.celrep.2018.10.080 (2018).

63 Pinder, A. G., Rogers, S. C., Khalatbari, A., Ingram, T. E. & James, P. E. The measurement of nitric oxide and its metabolites in biological samples by ozone-based chemiluminescence. *Methods in molecular biology (Clifton, N.J.)* **476**, 11-28 (2008).

64 Rogers, S. C. *et al.* Effect of plasma processing and storage on microparticle abundance, nitric oxide scavenging, and vasoactivity. *Transfusion* **59**, 1568-1577, doi:10.1111/trf.15214 (2019).

65 Bolger, A. M., Lohse, M. & Usadel, B. Trimmomatic: a flexible trimmer for Illumina sequence data. *Bioinformatics* **30**, 2114-2120, doi:10.1093/bioinformatics/btu170 (2014).

66 Zhu, Y. *et al.* Proteogenomics produces comprehensive and highly accurate protein-coding gene annotation in a complete genome assembly of *Malassezia sympodialis*. *Nucleic Acids Research* **45**, 2629-2643, doi:10.1093/nar/gkx006 (2017).

67 Pertea, M., Kim, D., Pertea, G. M., Leek, J. T. & Salzberg, S. L. Transcript-level expression analysis of RNA-seq experiments with HISAT, StringTie, and Ballgown. *Nat Protoc* **11**, 1650-1667, doi:10.1038/nprot.2016.095 (2016).

68 Afgan, E. *et al.* The Galaxy platform for accessible, reproducible, and collaborative biomedical analyses: 2018 update. *Nucleic Acids Research* **46**, W537-W544, doi:10.1093/nar/gky379 (2018).

69 Conesa, A. *et al.* Blast2GO: a universal tool for annotation, visualization, and analysis in functional genomics research. *Bioinformatics* **21**, 3674-3676, doi:10.1093/bioinformatics/bti610 (2005).

70 Kabsch, W. XDS. *Acta Crystallographica Section D* **66**, 125-132, doi:doi:10.1107/S0907444909047337 (2010).

71 McCoy, A. J. *et al.* Phaser crystallographic software. *Journal of Applied Crystallography* **40**, 658-674, doi:doi:10.1107/S0021889807021206 (2007).

72 Winn, M. D. *et al.* Overview of the CCP4 suite and current developments. *Acta crystallographica. Section D, Biological crystallography* **67**, 235-242, doi:10.1107/s0907444910045749 (2011).

73 Cowtan, K. Recent developments in classical density modification. *Acta crystallographica. Section D, Biological crystallography* **66**, 470-478, doi:10.1107/S090744490903947X (2010).

74 Arnold E, H. D., and Rossmann MG. *International Tables for Crystallography. Volume F: Crystallography of biological macromolecules.* 2nd edn, Vol. Volume F: (Kluwer Academic Publishers, 2012).

75 Afonine, P. V. *et al.* Towards automated crystallographic structure refinement with phenix.refine. *Acta crystallographica. Section D, Biological crystallography* **68**, 352-367, doi:10.1107/S0907444912001308 (2012).

76 Adams, P. D. *et al.* PHENIX: a comprehensive Python-based system for macromolecular structure solution. *Acta Crystallographica Section D* **66**, 213-221, doi:doi:10.1107/S0907444909052925 (2010).

77 Emsley, P., Lohkamp, B., Scott, W. G. & Cowtan, K. Features and development of Coot. *Acta crystallographica. Section D, Biological crystallography* **66**, 486-501, doi:10.1107/s0907444910007493 (2010).

78 Chen, V. B. *et al.* MolProbity: all-atom structure validation for macromolecular crystallography. *Acta crystallographica. Section D, Biological crystallography* **66**, 12-21, doi:10.1107/s0907444909042073 (2010).

79 Berman, H. M. *et al.* The Protein Data Bank. *Nucleic Acids Res* **28**, 235-242, doi:10.1093/nar/28.1.235 (2000).

80 Berman, H., Henrick, K. & Nakamura, H. Announcing the worldwide Protein Data Bank. *Nat Struct Biol* **10**, 980, doi:10.1038/nsb1203-980 (2003).

81 Pettersen, E. F. *et al.* UCSF Chimera--a visualization system for exploratory research and analysis. *Journal of computational chemistry* **25**, 1605-1612, doi:10.1002/jcc.20084 (2004).

82 O'Meara, T. R., Holmer, S. M., Selvig, K., Dietrich, F. & Alspaugh, J. A. *Cryptococcus neoformans* Rim101 is associated with cell wall remodeling and evasion of the host immune responses. *MBio* **4**, doi:10.1128/mBio.00522-12 (2013).

83 Laubach, V. E., Shesely, E. G., Smithies, O. & Sherman, P. A. Mice lacking inducible nitric oxide synthase are not resistant to lipopolysaccharide-induced death. *Proc Natl Acad Sci U S A* **92**, 10688-10692, doi:10.1073/pnas.92.23.10688 (1995).

84 Sparber, F. & LeibundGut-Landmann, S. Infecting mice with *Malassezia spp.* to study the fungus-host interaction. *Journal of visualized experiments : JoVE* (2019). http://europepmc.org/abstract/MED/31762452 https://doi.org/10.3791/60175.

85 Cossarizza, A. & al, e. Guidelines for the use of flow cytometry and cell sorting in immunological studies (second edition). *European Journal of Immunology* **49**, 1457-1973 (2019).

86 Overbergh, L. *et al.* The use of real-time reverse transcriptase PCR for the quantification of cytokine gene expression. *Journal of Biomolecular Techniques* **14**, 33-43 (2003).

87 Trautwein-Weidner, K., Gladiator, A., Nur, S., Diethelm, P. & LeibundGut-Landmann, S. IL-17-mediated antifungal defense in the oral mucosa is independent of neutrophils. *Mucosal immunology* **8**, 221-231, doi:10.1038/mi.2014.57 (2015).

88 Letunic, I. & Bork, P. Interactive tree of life (iTOL) v3: an online tool for the display and annotation of phylogenetic and other trees. *Nucleic Acids Res* **44**, W242-245, doi:10.1093/nar/gkw290 (2016).